RESOURCE ALLOCATION FOR INTERFERING MIMO LINKS

A Dissertation
Presented to
The Academic Faculty

by

Mehmet Fatih Demirkol

In Partial Fulfillment
of the Requirements for the Degree
Doctor of Philosophy in the
School of Electrical and Computer Engineering

Georgia Institute of Technology
April 2003

RESOURCE ALLOCATION FOR INTERFERING MIMO LINKS

Approved by:

Mary Ann Ingram, Committee Chair

Raghupathy Sivakumar

Ye (Geofferey) Li

Date Approved

TABLE OF CONTENTS

LIST OF TABLES

LIST OF FIGURES

LIST OF ABBREVIATIONS

ACK	$\triangleq$	Acknowledgement
AWGN	$\triangleq$	Additive White Gaussian Noise
BER	$\triangleq$	Bit-Error Rate
CCI	$\triangleq$	Cochannel Interference
CDF	$\triangleq$	Cumulative Distribution Function
CL	$\triangleq$	Closed-Loop
CL-I	$\triangleq$	CL-MIMO with Interference
CLT	$\triangleq$	Central Limit Theorem
CL-MIMO	$\triangleq$	Closed-Loop MIMO
CSI	$\triangleq$	Channel State Information
CTS	$\triangleq$	Clear-To-Send
DCF	$\triangleq$	Distributed Coordination Function
DIFS	$\triangleq$	Distributed Inter-Frame Spacing
DOFs	$\triangleq$	Degrees Of Freedom
FDD	$\triangleq$	Frequency-Division-Duplex
INR	$\triangleq$	Interference-to-Noise Ratio
LOS	$\triangleq$	Line-of-sight
MAC	$\triangleq$	Multiple-Access Control
MIMO	$\triangleq$	Multiple-Input Multiple-Output
MEA	$\triangleq$	Multi-Element Array
ML	$\triangleq$	Maximum Likelihood
MMSE	$\triangleq$	Minimum Mean-Square Error
MSE	$\triangleq$	Mean Square Error
MUD	$\triangleq$	Multiuser Detection
NLOS	$\triangleq$	Non-line-of-sight

OL	$\triangleq$	Open-Loop
OL-MIMO	$\triangleq$	Open-Loop MIMO
PDF	$\triangleq$	Probability Density Function
QoS	$\triangleq$	Quality of Service
RF	$\triangleq$	Radio Frequency
SIC	$\triangleq$	Successive Interference Cancellation
SIFS	$\triangleq$	Short Inter-Frame Spacing
SISO	$\triangleq$	Single-Input Single-Output
SVD	$\triangleq$	Singular-Value Decomposition
RTS	$\triangleq$	Request-To-Send
SNR	$\triangleq$	Signal-to-Interference Ratio
SNR	$\triangleq$	Signal-to-Noise Ratio
SNR	$\triangleq$	Time-Division-Duplex
TDMA	$\triangleq$	Time-Division Multiple-Access
ULA	$\triangleq$	Uniform Linear Array
ZF	$\triangleq$	Zero-Forcing

SUMMARY

Multiple-input multiple-output (MIMO) links are well known to provide high spectral efficiencies in rich multipath environments through the use of multiple spatial channels in the same system bandwidth. In rich scattering, the capacity is known to scale linearly with the number of transmitter and receiver antennas.

Traditionally, if two wireless links would cause excessive interference on each other, they are assigned to different channels, e.g. they could be time-multiplexed. If the links are both MIMO, however, the spatial filtering capabilities at both ends enable the MIMO links to operate co-channel with a higher network throughput than if they operated in a time-division multiple access (TDMA) fashion.

Closed-loop MIMO (CL-MIMO) uses channel-dependent matrix transformations (i.e. adaptive spatial filtering) at both the transmitter and the receiver to decompose the matrix channel into a collection of uncoupled parallel channels. The prefiltering at the transmitter is especially valuable in the presence of interference, at low signal-to-noise ratio (SNR), or in correlated fading. Thus, the throughput improvement with interfering MIMO links is realizable with closed-loop operation.

With interfering CL-MIMO links, the optimum link parameters are mutually dependent, since the transmit weights of one link effect the interference seen by another, which is not white. Thus, the optimal link parameters cannot be calculated independently at each link.

With ad hoc networks as the motivating application, this dissertation presents new resource allocation algorithms at the physical layer that allow interfering MIMO links to operate simultaneously. Distributed power- and capacity-controlled algorithms yield (sub)optimal transmit and receive weights for interfering CL-MIMO

links, and a stream control algorithm, also distributed, assures that the receivers are not overloaded with excessive desired and interference streams. Using transmit power, desired capacities, or the number of parallel streams for each link as control parameters, these algorithms produce higher network throughputs through spatial multiplexing than possible with TDMA. Moreover, these parameters allow control of the capacity of each link according to different data rate or quality of service (QoS) requirements.

One drawback of these algorithms is the required feedback of the channel state information (CSI) to the transmitter. CSI aging degrades CL-MIMO performance over time. When OL- and CL-MIMO performances are close, which is the case for high SNR links without interference or correlated fading, then high update rates are required to keep CL-MIMO performance above that of OL-MIMO. However, this dissertation shows that the difference between closed- and open-loop operation when links interfere is usually large. This implies that less frequent CSI updates will be sufficient to keep CL-MIMO performance above OL-MIMO.

The other drawback of these algorithms is the iterative joint adaptation of the link parameters. Each iteration requires a CSI update. Simulation results show that the most improvement takes place in the first few iterations. However, the overhead of CSI updates multiplied by the number of iterations may limit closed-loop operation to only static and low-mobility environments, such as indoor applications.

Assuming that the interference is white can eliminate the iterations; however, this assumption is not optimal. With this simplification and our stream control algorithm, spatial multiplexing gives an improvement over TDMA on the average. However, the performance with this solution can be worse than TDMA in some cases.

The algorithms are tested on both simulated and measured indoor MIMO channels. The dissertation presents what is apparently the first analysis of MIMO interference based on measured channels. This analysis shows the effects of environmental

factors, such as spatial correlation of desired and interference signals and disparate path losses, on the performance of the resource allocation algorithms.

This research gives an in-depth understanding of the flexibility and performance enhancement that MIMO links can provide, and the challenges they bring for an effective utilization of the resources in a network. The physical layer algorithms provide distributed resource allocation methods that can be used by future multiple-access control (MAC) layer designs.

CHAPTER 1

INTRODUCTION

This dissertation addresses the problem of joint adaptation of link parameters for a set of flat-fading cochannel multiple-input multiple-output (MIMO) links. We will show that with optimized parameters, interfering MIMO links can operate with a higher network throughput than if they operated in a time-division multiple-access (TDMA) fashion. These parameters include not only the transmit weight vectors and power for each stream, but also and perhaps more importantly, the number of independent data streams. With ad hoc networks as our motivating application, we develop distributed physical layer algorithms that allow *interfering* MIMO links to operate simultaneously. These algorithms can be viewed as distributed resource allocation methods which might be used by future multiple-access control (MAC) layer designs.

Rapid strides have been made in antenna array technology for wireless communications, particularly for links that have multi-element arrays (MEAs) at both ends. Concurrently, the speed and density of integrated circuit technology continues to increase. These facts have led equipment manufacturers to begin considering the use of MEAs on all sorts of user platforms that were not previously considered because of their cost, from homes for fixed wireless access to laptops and hand-held devices for indoor and picocell wireless networks [77].

MIMO links are well known to provide extremely high spectral efficiency in rich multipath environments through the use of multiple spatial channels in the same system bandwidth. Multiple data streams are transmitted in parallel on the same frequency band from one node. Thus, a link with a high signal-to-noise ratio (SNR)

is partitioned into many low-SNR subchannels. In rich scattering, the capacity of a wireless link scales linearly with the number of transmitter and receiver antennas if the fades between pairs of transmit-receive antennas are independent and identically distributed [25, 53, 70].

There are two categories of MIMO: open-loop (OL-MIMO), which requires no channel state information (CSI) at the transmitter, and closed-loop MIMO (CL-MIMO), which requires CSI at the transmitter.

1.1 Motivations and Challenges

The research presented in this dissertation has two main goals:

- **Improving the network throughput:** By employing cochnannel CL-MIMO links, we exploit the spatial filtering capabilities of MEAs at both ends of a link, and obtain higher network throughputs through spatial multiplexing than possible with TDMA.

- **Differential quality of service (QoS):** We present algorithms and parameters that can be used to allocate the wireless resources to the links in the network and to control the capacity of each link according to different data rate or QoS requirements.

The control parameters can be used by the higher (MAC) layer to fully exploit the physical layer. The appropriate MAC layer design would be different from the current standards, such as 802.11, which enforces time sharing among links that would interfere.

When antennas have independent fading and for high SNR, OL- and CL-MIMO approaches yield nearly equal capacities [58]. This result and the network overhead required to provide CSI to a transmitter have led to OL-MIMO receiving a great amount of attention in the literature. In most of these studies, single isolated links

are considered [14,24,25,31,34,35]. In a few more recent studies, effects of interference on the MIMO link performance is investigated [6, 9, 12, 39].

We investigate what levels of performances are possible in an ad hoc network where every node has a MEA and full software control of the transmitted and received signals. Next, we explain the motivations for and challenges of employing CL-MIMO links, a multiple access scheme that allows multiple cochannel links, and ad hoc networks.

1.1.1 CL-MIMO Links

If no channel information is available at the transmitter, the maximum mutual information is achieved if each transmitter antenna uses equal power and rate [25, 70]. Unless high complexity (two-dimensional) coding is used, the achievable data rate for an OL-MIMO link is limited by the stream with the least favorable channel.

CL-MIMO has higher spectral efficiency especially at low SNR, in the presence of interference [12, 18, 19], or in correlated fading [59]. If MIMO becomes common in wireless networks, then it will certainly operate in interference-limited environments, where CL may become worthwhile. This result motivates us to use power allocation strategies to exploit the spatial flexibility of MEAs. We elaborate on the interference issue separately.

CL-MIMO links require CSI at the transmitter as well as the receiver. The transmitter can obtain CSI only at certain time intervals, through feedback, or, in time-division-duplex (TDD) systems with no interference, through reception of signals in the reverse channel. We will assume that the transmitter gets explicit feedback from the receiver.

In a fading environment with rapid CSI aging, the transformation used at the transmitter to uncouple the parallel streams and the optimum power allocation may not match the channel realization for the duration of a packet transmission. In this

case, the closed-loop operation is not feasible.

With isolated MIMO links closed-loop operation is not feasible unless the channel is static. However, under interference conditions this is not the case. We show that our model of interfering CL-MIMO links perform better than OL-MIMO links even with moderate mobility.

1.1.2 Interfering Links

In this dissertation we consider a network with sets of cochannel MIMO links. A MIMO link can devote degrees of freedom in both its transmitter and receiver to achieving a high capacity, while limiting the interference caused at the receivers of other links.

Figure 1 depicts two interfering MIMO links with disparate QoS requirements. Each node has four antennas. The link with the higher QoS (Tx1-Rx1) uses three parallel streams, while the second link (Tx2-Rx2) uses one. Thus, the second link devotes more of its transmitter resources to avoid making interference on the high QoS link, and as well as its receiver resources to suppress the interference caused by the high QoS link. The parameters that control the links' resources can include transmit powers, desired link capacities, and the number of parallel streams.

It will be shown that simultaneous operation of cochannel MIMO links produces higher network throughputs than a TDMA scheme. In spite of the capacity reduction in a particular link because of interference from other co-channel links, the overall utilization of the channel is enhanced. The throughput improvement with respect to TDMA is demonstrated using both simulated channels and indoor channel measurements for different network topologies.

One challenge of employing cochannel MIMO links is that the data rate and transmit power are distributed to each link, as well as to each data stream of a link. We will show that the network throughput can sometimes be improved if fewer than

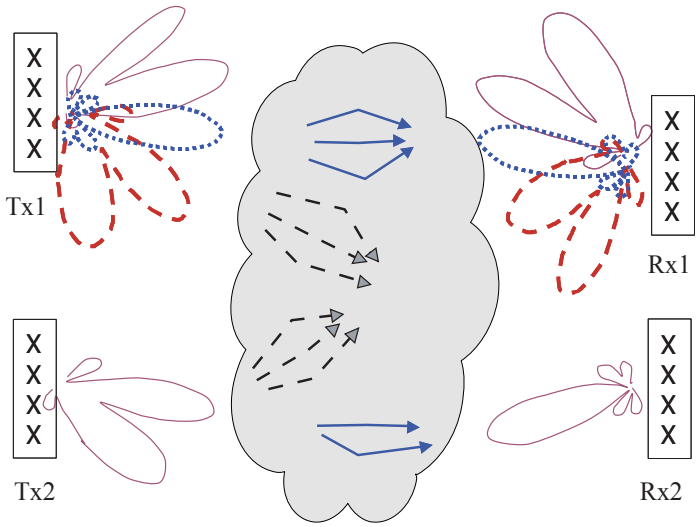

Figure 1: Interfering MIMO links.

the maximum number of streams are transmitted; this we call stream control. The cost functions used to optimally allocate the resources for each link are not simply the SNR or signal-to-interference ratio (SIR). Shannon's channel capacity is used as a measure of the data-carrying capability of each MIMO link.

Moreover, with CL-MIMO links, the optimum transmit weights and power allocation parameters are not independent for each link. The capacity of each link and its optimum transmit-signal correlation matrix are functions of the channel and the external interference at the receiver. Since the external interference is affected by the transmitter correlation matrices of the interfering transmitters, the optimum transmission strategies and the capacities of all links are mutually dependent. As a result, the link parameters cannot be calculated independently at each link. Iterative methods are used to jointly optimize the optimal transmit and receive transformations.

1.1.3 Ad hoc Networks

Ad hoc networks are multi-hop wireless networks that lack the services of an established backbone infrastructure. The mobile stations in the network function as forwarders and participate in the routing process.

With the tendency to extend wireless coverage and to reduce infrastructure costs, ad hoc and multi-hop networks have gained importance. Such networks are finding applications even in commercial wireless packet data environments.

We consider ad hoc networks, where there is no central control of data transmissions, and all nodes have similar characteristics. However, the algorithms and results presented are also applicable to cellular networks with appropriate changes in the modelling of the wireless channel and resources at the base station.

The main challenge of employing an ad hoc network is that all algorithms need to be distributed. This creates difficulties in the stream control problem addressed in Chapter 4. However, global numerical optimization of all antenna weights to optimize network throughput is computationally prohibitive even if the channel gains between all pairs of nodes are centrally gathered. The simplicity and the fast convergence of the distributed link adaptation algorithms introduced in Chapter 3 make them attractive even for centrally-controlled network systems.

1.2 Dissertation Outline

The rest of this dissertation is organized as follows: Chapter 2 presents background material and concepts related to the proposed research.

In Chapter 3 the problem of joint link adaptation for interfering MIMO links is discussed, and two distributed iterative algorithms that complement each other are proposed. The first algorithm gives optimal link capacities based on total transmit powers, while the second gives transmit powers necessary to meet capacity constraints.

In Chapter 4 it is shown that the distributed algorithms do not necessarily maximize the total network throughput. A modification to the distributed algorithms is proposed in to limit the number of streams transmitted by each link so that the receiver nodes are not overloaded with excessive number of streams. An algorithm to distributively control the number of streams in the overload condition is also given.

Chapters 5 and 6 demonstrate the throughput improvement of the new physical layer model with interfering MIMO links and the distributed link adaptation algorithms for different network topologies. Chapter 5 uses simulated channels and Chapter 6 uses measured channels.

Chapter 7 discusses some practical issues such as CSI aging and the overhead of iterative joint link adaptation. Noniterative suboptimal solutions to the joint link adaptation problem are given, and their performances are demonstrated.

Finally, Chapter 8 summarizes main contributions of this dissertation and lists possible future research directions.

CHAPTER 2

BACKGROUND

The necessary background knowledge is reviewed and some key concepts are introduced in this chapter. In Section 2.1 we summarize the main properties of ad hoc networks and MAC protocol particularly for the IEEE 802.11 standard. Section 2.2 introduces some fundamental concepts of antenna arrays. Section 2.3 summarizes MEA transmission strategies. In Section 2.4 we formulate the MIMO channel capacity. The water-filling solution is given assuming additive Gaussian noise and interference. In Section 2.5 we introduce the channel models used for our simulations. Statistics of the channel mode gains and MIMO capacity are reviewed in Section 2.6. Bounds on the MIMO capacity are reviewed, and a Gaussian approximation is given. Sections 2.7 and 2.8 overview the methods of MIMO channel tracking and CSI feedback to the transmitter, respectively. Brief discussions of the OL-MIMO architectures considered in the literature, and the performance with CL-MIMO links are given in Sections 2.9 and 2.10. The last section summarizes the problem of joint optimization of cochannel links, and explains how the problem changes if the links are MIMO.

2.1 Ad Hoc Networks and MAC protocol of IEEE 802.11 Standard

We are primarily interested in distributed algorithms that can be used by ad hoc networks. A popularly used MAC scheme in wireless ad hoc networks is the distributed coordination function (DCF) mode of the IEEE 802.11 standard. The baseline of comparison for the new algorithms will be the 802.11 standard in the DCF mode. Therefore, we give a brief discussion of the ad hoc networks and the MAC protocol

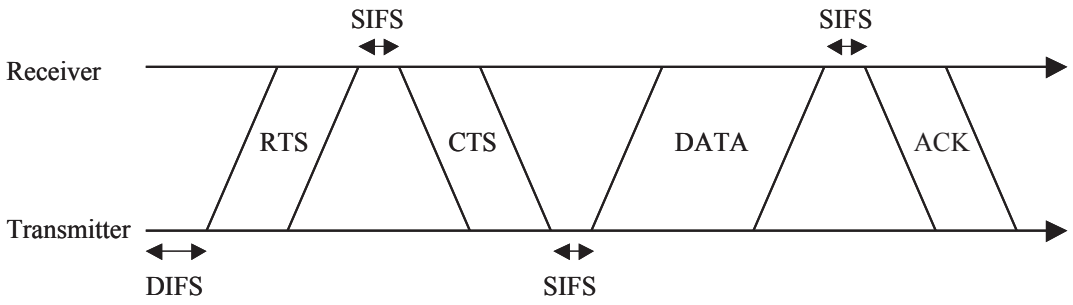

Figure 2: Four-way handshake of CSMA/CA.

of 802.11.

Ad hoc networks are multi-hop wireless networks that with no fixed infrastructure and no centralized administration. The mobile stations in the network function as forwarders and participate in the routing process. Nodes communicate by creating a network "on the fly," and the topology can change as the nodes move.

The MAC layer is responsible for fair and orderly use of the shared medium. The MAC protocol used in the IEEE 802.11 standard is carrier-sense multiple-access with collision avoidance (CSMA/CA). In this protocol, a node with a packet to be transmitted first listens to ensure no other node is transmitting. If the channel is clear, it transmits the packet. Otherwise, it backs off, and tries again later. The back-off time is randomized to minimize the collisions between packets. When the channel is detected vacant by the carrier-sense method, the transmitter first sends a request-to-send (RTS) message. The recipient answers with a clear-to-send (CTS), if it is not contending. This exchange of control packets aims to ensure collision-free transmission of the data. The transmission of the data packet (DATA) is followed by an acknowledgement (ACK) by the receiver. If the transmitter does not hear the ACK, the data is retransmitted [52]. This four-way handshake is summarized in Figure 2. In the figure, SIFS and DIFS stand for short and distributed inter-frame spacings, respectively.

Suppose each of two nodes have packets to be sent to different receivers in a

network. With the TDMA-based MAC protocol described above, each transmitter would try to gain access to the channel, and only one link would be active at all times. However, with MEAs at all nodes, another MAC protocol that exploits the spatial filtering capabilities of the arrays might yield higher throughput.

Several recent studies have proposed modifications to 802.11 for use with MEAs [4, 41, 51]. However, these studies are based on directional and single-stream transmission.

The physical layer algorithms presented in this dissertation assume fully adaptive antenna arrays at both ends of the link, and allow sets of cochannel CL-MIMO links to operate simultaneously.

2.2 Antenna Arrays

MEAs, or antenna arrays, are vital to high-capacity communications system development [29, 55, 72–74]. Antenna arrays can be used to increase channel capacity and spectrum efficiency; extend range of coverage; and reduce transmit power, co-channel interference, multipath fading, bit-error rate (BER), and outage probability. Antenna arrays are also used for radar operation and in military applications such as direction finding and nulling out enemy interferers [47].

A typical antenna array consists of equispaced omnidirectional elements. The array can also have orthogonally polarized elements to provide polarization diversity, and the geometry of the array can vary. However, the most common configurations are linear or circular arrays [71]. The desired receive or transmit pattern can be formed by adjusting the array weights.

A node with a MEA containing M elements is said to have M *degrees of freedom* (DOFs). These DOFs correspond to the constraints that can be satisfied through linear combination of array inputs or outputs. If a node is receiving, these DOFs can be used to provide power gain of M over white noise, null up to $M-1$ interferers,

or receive up to M parallel streams. Similarly, a transmitter node can use its DOFs to provide a power gain by concentrating its transmission power in beams, to avoid transmitting interference to certain directions, or to transmit multiple streams in parallel.

2.3 MEA Transmission Strategies

A variety of MEA transmission strategies have been considered in combination with the MEA reception techniques, creating strategies for MIMO links. The MEA transmission strategies for transmission of a single data stream include beam switching or steering [23, 45] and adaptive arrays [23]. For transmission of multiple data streams, there is transmit diversity [2] and spatial multiplexing [25, 53].[1] While these techniques each have their respective advantages and disadvantages, which are discussed below, spatial multiplexing stands out for the remarkable spectral efficiencies that it produces in rich scattering environments [24, 53].

2.3.1 Beam Switching and Beam Steering

In beam switching or steering, a weight vector is designed without regard to the specific channel conditions. An array pattern is produced according to the desired characteristics, such as a mainlobe with a desired beamwidth and a certain sidelobe roll-off. By modifying the phases of the antenna weights the mainlobe can be steered to a desired angle. This transmission strategy mimics the mechanical steering of a directional antenna, such as a dish. Ideally, beam steering implies a continuum of possible steering angles, whereas beam switching implies a finite set of possible angles. A single data stream is transmitted out of the array. Figure 3(a) shows example array patterns associated with beam steering.

The advantages of beam switching or steering are (1) that the weight and steering

[1] Transmit diversity is listed as a "multiple data stream" method because as a source of interference it appears this way to other links.

vectors can be implemented in analog radio frequency (RF) hardware, implying that only one radio chain (RF-to-baseband conversion) is needed, (2) the directionality of the array pattern puts high gain in the desired direction (assumed known) and low gain in the directions of interference signals, and (3) only a single parameter (desired signal direction) is needed by the transmitter to steer the beam. However, the disadvantages are: (1) Careful array calibration is needed to ensure pattern characteristics. (2) To have an appreciable benefit from a conventional beam, the array must have enough elements. For example, for indoor environments, 8 elements are needed [45]. (3) Channel gain is lost if the angular spread of the desired signal multipath is larger than the mainlobe width [75].

2.3.2 Adaptive Array

An adaptive array is similar to beam steering in that a single data stream is transmitted using all elements of the array. However, in the adaptive array, the weight vector depends on the multipath fading of the channel; in particular, it is the principal right singular vector of the channel matrix, and therefore, will not generally have a single mainlobe and low side lobes, as shown in Figure 3(b).

The adaptive array may be considered as a type of transmit diversity, since it involves redundant transmission of data across array elements. It's advantages are (1) that it provides diversity gain, (2) the interference produced by an adaptive array is not so difficult to suppress because it is a single data stream [8], and (3) optimal combining at the receiver is simpler than for space-time coding. Some disadvantages are (1) channel information is required at the transmitter and (2) full diversity gain will not be achieved for channels with rank higher than one.

2.3.3 Transmit Diversity

Transmit diversity is a space-time coding technique in which data is spread redundantly across transmit antenna elements to make a link reliable in the presence of

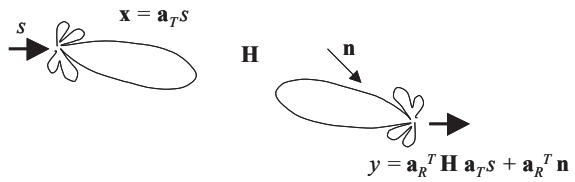

(a) Beam steering.

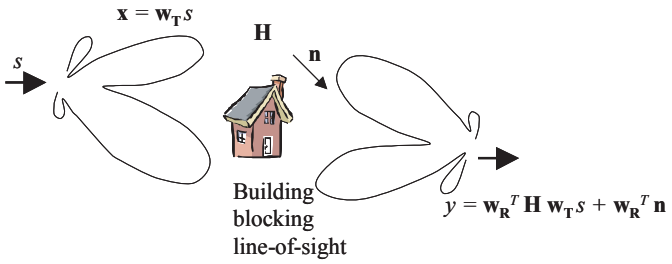

(b) Adaptive array.

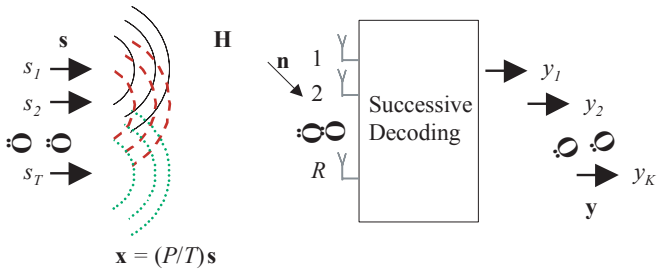

(c) Open-loop spatial multiplexing.

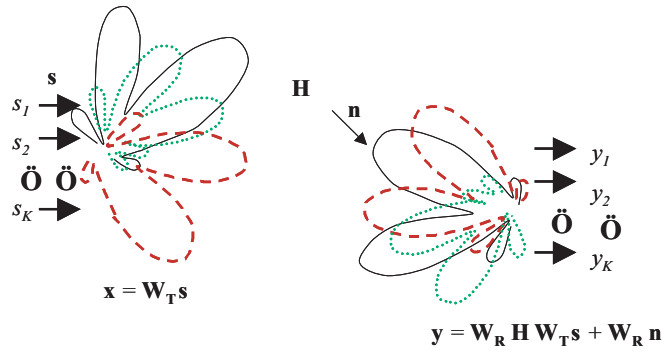

(d) Closed-loop spatial multiplexing.

Figure 3: Illustrations of array patterns for various transmit strategies.

multipath fading. Transmit diversity is particularly useful when the transmitter does not have the channel knowledge and the channel is not reliable. Alamouti proposed a simple block code for transmission using two antennas [2]. Other techniques include the layered space-time scheme of Foschini [24][2] , the space-time trellis codes [69] and the generalized space-time block codes [67, 68] by Tarokh *et al.* Some studies have considered cooperation of multiple nodes to exploit transmit diversity [42, 57]. Note that Foschini's architecture [24] is a spatial multiplexing scheme, since multiple streams are transmitted. However, in this diagonally coded architecture there is coding dependency among the streams transmitted from each antenna; therefore, transmit diversity is exploited.

The advantages of transmit diversity include (1) that no channel information is required at the transmitter and (2) that the receiver need not have multiple antenna elements to benefit from the diversity gain. Disadvantages include (1) that an interference source using transmit diversity creates a number of interference data streams equal to the number of transmit antenna elements, which is a more difficult type of interference to suppress, (2) a separate radio chain is required for each transmit antenna element, and (3) the achievable data rates are low compared to the rates that can be achieved by spatial multiplexing.

2.3.4 Spatial Multiplexing

Finally, in MIMO links, multiple data streams are transmitted in parallel. A simple application of this kind is formed in a multiple-access cellular network with MEAs at the base stations and single antennas at the mobiles. Another application that has more recently gained interest, and particularly studied here, is formed by links with MEAs at both the transmitter and the receiver. When all transmitting antennas are

[2]Althouth multiple streams are transmitted in parallel with this scheme, the original diagonal architecture of [24] is also a transmit diversity technique, since there is coding dependency between the antenna elements.

at a single node, coordination between the transmitted streams is possible.

In *open-loop* spatial multiplexing, channel condition is not exploited at the transmitter and each antenna element transmits a different data stream with equal power. This is illustrated in Figure 3(c). In *closed-loop* spatial multiplexing, both the transmitter and the receiver adapt to the channel conditions. Each stream has corresponding transmit and receive antenna patterns as depicted in Figure 3(d).

We note that the adaptive array method discussed previously is a special case of the closed-loop spatial multiplexing scheme, where only the strongest channel mode is used.

Spatially multiplexed or MIMO links have received a great deal of attention because of the tremendous spectral efficiencies that can be achieved because of their parallel nature. Specifically, the well-known result (and the great advantage of this approach) is that the capacity increases linearly with the number of transmit and receive antennas in a rich multipath environment [25]. Often, indoor wireless networks, terrestrial military and emergency relief networks have rich multipath channels. The disadvantages are (1) that radio chains are required for all antenna elements and in the closed-loop case, (2) channel information is required at the transmitter, and (3) variable power and bit loading requires more computing complexity at the transmitter than for the other methods.

Because of this high efficiency, we will study the link adaptation and performance of networks with MIMO links. In the next section we look at the MIMO channel capacity and study the MIMO links in more detail.

2.4 MIMO Channel Capacity

A MIMO link uses multiple spatial channels to increase the data rate while maintaining reliable data detection at the receiver. A useful measure of the data-carrying capability of such a system is Shannon's channel capacity. This is the maximum rate

of information that can be sent essentially error free across the channel.

In this section, the MIMO communication system is introduced, and formulation of the channel capacity is given. First, some fundamental definitions of information theory that lead to the channel capacity are provided.

2.4.1 Entropy, Mutual Information, Capacity, and Signalling

Entropy is a measure of the degree of uncertainty for a discrete memoryless source. It gives the average information content per source per symbol. For a continuous random variable, we define *differential entropy*. For a continuous random vector $\mathbf{X}$ with joint probability density function $f_{\mathbf{X}}(\mathbf{x})$, the differential entropy is

$$h(\mathbf{X}) = \int_{-\infty}^{\infty} f_{\mathbf{X}}(\mathbf{x}) \log_2 \left[\frac{1}{f_{\mathbf{X}}(\mathbf{x})} \right] d\mathbf{x} \tag{1}$$

Mutual information between $\mathbf{X}$ and $\mathbf{Y}$ measures the reduction in uncertainty about $\mathbf{X}$ that results from learning $\mathbf{Y}$, or vice-versa. It is given by

$$\begin{aligned} I(\mathbf{X};\mathbf{Y}) &= h(\mathbf{X}) - h(\mathbf{X}|\mathbf{Y}) & (2) \\ &= \int_{-\infty}^{\infty} \int_{-\infty}^{\infty} f_{\mathbf{X},\mathbf{Y}}(\mathbf{x},\mathbf{y}) \log_2 \left[\frac{f_{\mathbf{X}}(\mathbf{x}|\mathbf{y})}{f_{\mathbf{X}}(\mathbf{x})} \right] d\mathbf{x} d\mathbf{y} & (3) \end{aligned}$$

In this relation, $h(\mathbf{X}|\mathbf{Y})$ is the *conditional differential entropy* of $\mathbf{X}$ given $\mathbf{Y}$, $f_{\mathbf{X},\mathbf{Y}}(\mathbf{x},\mathbf{y})$ is the joint probability density function of $\mathbf{X}$ and $\mathbf{Y}$, and $f_{\mathbf{X}}(\mathbf{x}|\mathbf{y})$ is the conditional probability density function of $\mathbf{X}$, given that $\mathbf{Y} = \mathbf{y}$.

The *information capacity* of the MIMO channel is obtained by maximizing the mutual information between the channel input $\mathbf{X}$ and output $\mathbf{Y}$ over all distributions of $\mathbf{X}$, with a total transmit power constraint [15]. This is equivalent to maximizing the differential entropy of $\mathbf{Y}$, which requires that $\mathbf{Y}$, and consequently $\mathbf{X}$, are circularly symmetric complex Gaussian [33, 70].

The probability density of a circularly symmetric complex Gaussian with mean μ and covariance matrix $\mathbf{Q}$ is

$$f_{\mathbf{X}}(\mathbf{x}) = \det(\pi\mathbf{Q})^{-1} \exp\left[-(\mathbf{x}-\mu)' \mathbf{Q}^{-1} (\mathbf{x}-\mu) \right] \tag{4}$$

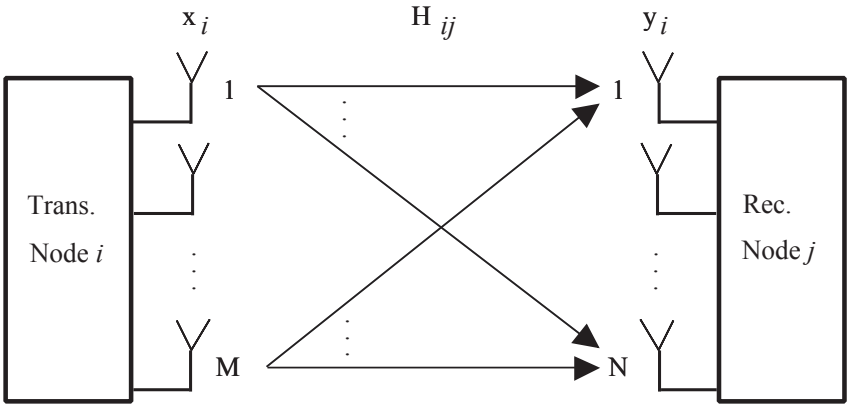

Figure 4: Block Diagram of a MIMO Link

The differential entropy for this random vector is given by

$$h(\mathbf{X}) = log_2|\pi e\mathbf{Q}| \tag{5}$$

2.4.2 MIMO Link

In Figure 4, a block diagram of a flat-fading MIMO link is given. The transmitter and receiver arrays have M and N elements, respectively.

Use of multiple antenna elements at both the transmitter and the receiver provides multiple parallel channels on the same frequency band. Therefore, a MIMO link provides high spectral efficiencies through partitioning of a single high-SNR link into many low-SNR subchannels. In rich scattering, capacity of an $N \times M$ MIMO link scales linearly with $\min(M, N)$ [24].

For this link, the output vector of the receiver antenna array is

$$\mathbf{y}_j = \mathbf{H}_{ij}\mathbf{x}_i + \mathbf{n}_j \tag{6}$$

where $\mathbf{x}_i$ denotes the transmitted signal vector, $\mathbf{n}_j$ is a vector of white Gaussian noise samples, and $\mathbf{H}_{ij}$ is the complex channel matrix between transmitter node i to receiver node j.[3] Each element $\mathbf{H}_{ij}(a, b)$ of the channel matrix gives the complex

[3]The subscript pair $\{ij\}$ may be omitted in some discussions involving only a single isolated MIMO link throughout this dissertation.

channel function from antenna element b of the transmitter to antenna element a of the receiver. The channel capacity for this system is

$$C_{ij} = \max_{\mathbf{P}_{ij}} \log_2 \frac{\left|\sigma_n^2 \mathbf{I} + \mathbf{H}_{ij}\mathbf{\Psi}_{ij}\mathbf{H}'_{ij}\right|}{\sigma_n^2}, \tag{7}$$

where $\mathbf{\Psi}_{ij}$ is the transmit-signal correlation matrix (with the assumption that $\mathbf{x}_i$ is zero-mean), or the power allocation matrix, and σ_n^2 is the power of the white Gaussian noise seen at each receiver antenna.

For simplicity, we define $\mathbf{P}_{ij} = \mathbf{\Psi}_{ij}/\sigma_n^2$, the noise-normalized power allocation matrix. Thus, the formula for the MIMO channel capacity becomes

$$C_{ij} = \max_{\mathbf{P}_{ij}} \log_2 \left|\mathbf{I} + \mathbf{H}_{ij}\mathbf{P}_{ij}\mathbf{H}'_{ij}\right|. \tag{8}$$

2.4.3 Open-Loop Capacity

In open-loop spatial multiplexing (OL-MIMO), no channel information is used at the transmitter and each antenna element transmits a different data stream with equal power. Specifically, setting $\mathbf{P}_{ij} = (P_{ij,T}/M)\mathbf{I}$ gives the best result [25, 70]. Here, $P_{ij,T}$ is the total transmitted power, normalized by the additive noise power. Thus, the channel capacity of OL-MIMO is

$$C_{ij} = \sum_{k=1}^{K_{ij}} \log_2 \left(1 + \frac{P_{ij,T}}{M}\lambda_{ij,k}\right) \tag{9}$$

where $\lambda_{ij,k}$, $k = 1, ...K_{ij}$ are the nonzero eigenvalues of $\mathbf{H}_{ij}\mathbf{H}'_{ij}$ in decreasing order.

The receive array employs a multi-user detection technique, such as successive interference cancellation [24], to separate and detect the data streams.

2.4.4 Closed-Loop Capacity

In closed-loop spatial multiplexing (CL-MIMO), channel-dependent matrix transformations in both the transmitter and receiver decompose the matrix channel into a collection of uncoupled parallel channels or *channel modes*. The output of each transmit antenna is a linear combination of the multiplexed signals.

Let the singular-value decomposition (SVD) of $\mathbf{H}_{ij}$ be denoted as $\mathbf{H}_{ij} = \mathbf{U}_{ij}\mathbf{S}_{ij}\mathbf{V}'_{ij}$ and the eigenvalue decomposition of $\mathbf{P}_{ij}$ as $\mathbf{P}_{ij} = \mathbf{D}_{ij}\mathbf{\Sigma}_{ij}\mathbf{D}'_{ij}$. Furthermore, let $\alpha_{ij,k}$, $k = 1, ...K_{ij}$ be the nonzero eigenvalues of $\mathbf{P}_{ij}$. With the choice of $\mathbf{D}_{ij} = \mathbf{V}_{ij}$, the expression for the capacity becomes [70]

$$C_{ij} = \max_{\alpha_{ij,k}} \sum_{k=1}^{K_{ij}} \log_2(1 + \lambda_{ij,k}\alpha_{ij,k}). \tag{10}$$

The classical water-filling solution

$$\alpha_{ij,k} = \left[\mu - \frac{1}{\lambda_{ij,k}}\right]^+, \tag{11}$$

maximizes the sum in (10) where $[\cdot]^+$ indicates that only nonnegative values are acceptable, and μ is chosen so that $\sum_{k=1}^{K_{ij}} \alpha_{ij,k} = P_{ij,T}$.

In summary, the power allocated to each independent stream is determined by (11), and the weights used at the transmitter and the receiver nodes are determined by the right and left singular vectors of the channel matrix, respectively.

2.4.5 Capacity with Interference

The water-filling approach can be modified to accommodate fixed nonwhite interference at the receiver of a link (represented by a noise-normalized covariance matrix, $\mathbf{R}$) by "whitening the channel matrix" first. Applying a spatial whitening transform to the channel yields

$$\widetilde{\mathbf{H}} = [\mathbf{I} + \mathbf{R}]^{-1/2}\,\mathbf{H}, \tag{12}$$

which reduces the capacity relation to the simple form in (8), with a substitution of $\mathbf{H} \rightarrow \widetilde{\mathbf{H}}$ [6]. Thus, the capacity formula becomes

$$C = \max_{\mathbf{P}} \log_2 \left|\mathbf{I} + \widetilde{\mathbf{H}}\mathbf{P}\widetilde{\mathbf{H}}'\right| \tag{13}$$

$$= \max_{\mathbf{P}} \log_2 \left|\mathbf{I} + (\mathbf{I} + \mathbf{R})^{-1}\,\mathbf{H}\mathbf{P}\mathbf{H}'\right|. \tag{14}$$

The whitening operation assumes linear processing to suppress interference. It is assumed that the interfering signals are unknown to the receiver and they are modelled

as Gaussian distributed. Only the spatial characteristic of the interference power is exploited. This formula for the capacity with interference is also used in [1, 21, 39].

Treating the interference as noise is optimal only if it is weak. It is shown in [16] that decoding of the interfering streams is preferable in the strong-interference case. Linear minimum mean-square error (MMSE) and successive interference cancellation (SIC) are shown to be effective multiuser detection (MUD) methods.

However, we use the whitening method and assume the worse case for the interference streams throughout this dissertation to limit the scope of our analysis by a single performance metric (capacity).

With the whitening transformation in (12) the optimum transmit strategy becomes a function of the received interference, $\mathbf{R}$, as well as the channel matrix, $\mathbf{H}$.

The whitening transformation degrades the channel by modifying the modes and robbing gain from them, so that the capacity of the link is less than it would be without the interference. In the infinite interference-to-noise case, whitening projects a square channel matrix onto a lower-dimensional subspace, thereby simply reducing the number of available modes by the number of interfering data streams [5].

2.5 Channel Model

Our general approach will be to use stochastic, flat-fading models and then to collect the statistics on our chosen performance metric, network throughput, which is the sum of the link capacities.

We use two different models for the computer simulation of mulipath fading channels: quasistatic and mobile. In a quasistatic environment the channel stays fixed for the duration of an entire burst. We use this model in the next three chapters, which treat link adaptation assuming both the transmitter and the receiver have perfect CSI. We use the mobile channel model in Chapter 7, which considers CSI aging.

We also demonstrate the performance of our algorithms using MIMO flat-fading

channels that were measured in the Residential Laboratory of Georgia Institute of Technology, which is like a home environment. The description of the measurements are given, along with the results, in Chapter 6.

In the remainder of this section the quasistatic and mobile MIMO channel models are introduced.

2.5.1 Quasistatic Model

For computer simulation of MIMO multipath-fading channels, we utilize a Rayleigh fading model. The separation between elements of the arrays at the transmitter and receiver are assumed to be large enough for the fades to be independent. Each entry of the channel is a zero-mean, independent and identically distributed Gaussian random variable that has independent real and imaginary parts with equal variance. Equivalently, the entries of the channel matrix have uniformly distributed phase and Rayleigh magnitude.

The channel gain depends on the distance, D, between the nodes. The mean-square value of each element of the channel matrix is equal to $1/D^n$, where n is the path-loss exponent. In the simulations, $n = 3$ is used. We will assume that the shadowing effect is the same for all antenna elements of a node and the shadowing coefficient is absorbed into the *noise-normalized transmit power*.

We consider MIMO links in ad hoc networks, where there are no base stations (BS), and both ends of a link are expected to be located in environments with similar scattering properties. Therefore, we assume that the fades of the array elements are decorrelated on both sides of a link, and we do not distinguish between uplink and downlink.

2.5.2 Mobile Model

As with the quasistatic model, we generate stationary, Rayleigh faded channels. Each element of the channel matrix is normalized by $1/D^n$ to account for the path loss.

We use the filtered Gaussian noise method to simulate a fading channel [63].

For simplicity, we use a first-order low-pass filter. Let $\mathbf{H}_{ij,p}$ represent the complex Gaussian random matrix sampled at time $p\tau$, where τ is the simulation step size and p is the time epoch. The state equation for the samples of the channel matrix is

$$\mathbf{H}_{ij,p+1} = \zeta \mathbf{H}_{ij,p} + (1-\zeta)\,\mathbf{G}_{ij,p} \tag{15}$$

where $\mathbf{G}_{ij,p}$ is a zero-mean complex Gaussian matrix with variance

$$\sigma^2 = \frac{1+\zeta}{1-\zeta}. \tag{16}$$

For a maximum Doppler spread of f_m the value of ζ is set to

$$\zeta = 2 - \cos(2\pi f_m T) - \sqrt{[2-\cos(2\pi f_m T)]^2 - 1}. \tag{17}$$

2.6 Statistics of the Channel Mode Gains and MIMO Capacity

Capacity depends on the channel mode gains, or the eigenvalues of the channel gain matrix, $\mathbf{HH}'$. With interfering CL-MIMO links, iterative methods are used to calculate the capacities. For distributed computation of some control parameters and for decisions of the MAC layer, obtaining the statistics of the channel mode gains and the channel capacity would be useful.

2.6.1 Distribution of the Channel Mode Gains

With the channel matrix $\mathbf{H}$ modelled as an $M \times N$ random matrix with iid complex Gaussian elements with zero mean and unit variance, we define

$$\mathbf{W} = \begin{cases} \mathbf{HH}', & M < N \\ \mathbf{H}'\mathbf{H}, & M \geq N \end{cases} \tag{18}$$

The Hermitian $m \times m$ random matrix, $\mathbf{W}$, has a complex Wishart multivariate distribution with parameters m and n [20,70], where $m = \min(M, N)$ and $n = \max(M, N)$. The channel mode gains, λ_k, are the eigenvalues of $\mathbf{W}$.

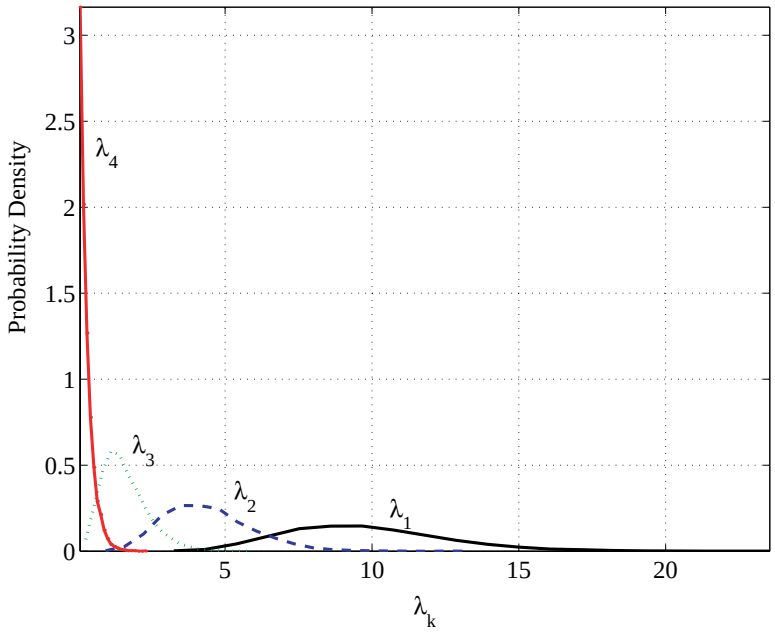

Figure 5: Distributions of the ordered channel mode gains, λ_k, for a 4×4 channel.

The joint density of the eigenvalues $\lambda_1 \geq \ldots \geq \lambda_m$ is given as [20, 70]

$$p_\lambda(\lambda_1, \ldots, \lambda_m) = \frac{2^{-mn}\pi^{m(m-1)}}{\Gamma_m(n)\Gamma_m(m)} \exp\left(-\sum_i \lambda_i\right) \prod_i \lambda_i^{n-m} \prod_{i<j} (\lambda_i - \lambda_j)^2 \tag{19}$$

where $\Gamma_m(n)$ is the complex multivariate gamma function.

Figure 5 shows sample probability density function (PDFs) of the ordered channel mode gains for a 4×4 channel.

The trace of $\mathbf{HH}'$, which is equal to the sum of the channel mode gains, is a central χ^2-distributed random variable with 2MN degrees of freedom.

The distributions for the largest and the smallest eigenvalues of $\mathbf{HH}'$ are studied in [20] for special values of m/n. We only summarize the asymptotic results for the more general case here. As m and n tend to infinity, the expected values of the maximum and the minimum eigenvalues of $\mathbf{W}(m, n)$ approach [20, 60]

$$\lambda_{\min} \to m\left(1 - \sqrt{\frac{m}{n}}\right)^2 \tag{20}$$

$$\lambda_{\max} \to \left(\sqrt{m} + \sqrt{n}\right)^2. \tag{21}$$

2.6.2 Statistics of the MIMO Channel Capacity

The statistics of the capacity for an isolated OL-MIMO are studied in [58, 61, 70]. To summarize some of the results, the mean of the capacity grows linearly with m and logarithmically with the total transmit power, P_T. The variance grows logarithmically with power, and in the limit of large P_T, also grows logarithmically with m. But in the limit of large number of antennas, the variance does not depend on m [58].

Although these results give us a general idea about the dependence of capacity on the transmit power and the number of antennas, they are too complex for practical use. Therefore, we review some bounds, and give a Gaussian approximation to the MIMO capacity.

2.6.3 Bounds on the MIMO Capacity

2.6.3.1 A Lower Bound

Foschini and Gans derive a lower bound on the OL-MIMO capacity [25]. With χ^2_{2k} denoting a chi-squared random variable with $2k$ degrees of freedom, the lower bound is given as

$$C_{\text{LB}} = K \sum_{k=1}^{K} \log_2 \left(1 + \frac{P_T}{M} \chi^2_{2k} \right). \tag{22}$$

2.6.3.2 An Upper Bound

An upper bound is given in [27] on the open-loop MIMO link capacity in (9). The upper bound uses the expected average of the channel mode gains. Each channel mode gain is replaced by $\frac{1}{K} \sum_{k=1}^{K} \lambda_k$. The bound is given as

$$C_{\text{UB}} = K \log_2 \left(1 + \frac{P_T}{MK} \sum_{k=1}^{K} \lambda_k \right). \tag{23}$$

The upper bound equals the actual capacity only if all eigenvalues of the channel matrix are equal, or if the rank of the channel matrix is one.

Given that the trace of $\mathbf{HH}'$, or the sum of the channel mode gains, is a central χ^2-distributed random variable with $2MN$ degrees of freedom, the distribution of this random variable is derived as [4]

$$\begin{aligned} p_X(x) &= \frac{\ln(2)}{K(MN-1)!}\left(\frac{KM}{P_T}\right)^{MN} \cdot \\ &\quad 2^{x/K}\left(2^{x/K}-1\right)^{MN-1}\exp\left[-\frac{KM}{P_T}\left(2^{x/K}-1\right)\right]\mathtt{u}(x), \end{aligned} \tag{24}$$

where $\mathtt{u}(x)$ is the unit step function.

2.6.4 Gaussian Approximation

We showed in [17] that the MIMO capacity can be modelled as Gaussian even for small number of antennas. Capacity does not have a Gaussian distribution, since it cannot be negative. However, for large number of transmit and receive antennas, it can be modelled as Gaussian.

According to the central limit theorem (CLT), the distribution of the MIMO capacity tends to Gaussian as the number of antennas at both ends of the link grows. For a single-input single-output (SISO) link, the capacity is given by

$$C_{SISO} = \log_2(1+P\lambda) \tag{25}$$

where λ is a chi-squared random variable when the channel coefficient is Rayleigh [25], and P is the noise-normalized transmission power. For nodes with N antennas, assuming the channel matrix has full rank, the capacity given by equation (10) is the sum of N terms similar to the expression in equation (25). This summation is the basis of the CLT argument.

Figure 6 shows the normal probability plots of the capacities for 1×1, 3×3, 4×4 and 8×8 isolated MIMO links. For each plot, 500 sets of channel samples are

[4]Note that this is slightly different from the expression in [27], because in [27] the variance of each complex Gaussian element of the channel matrix is 2, where we use unit variance throughout this dissertation. Equivalently, the real and imaginary components of each element of the channel matrix has variance 1/2.

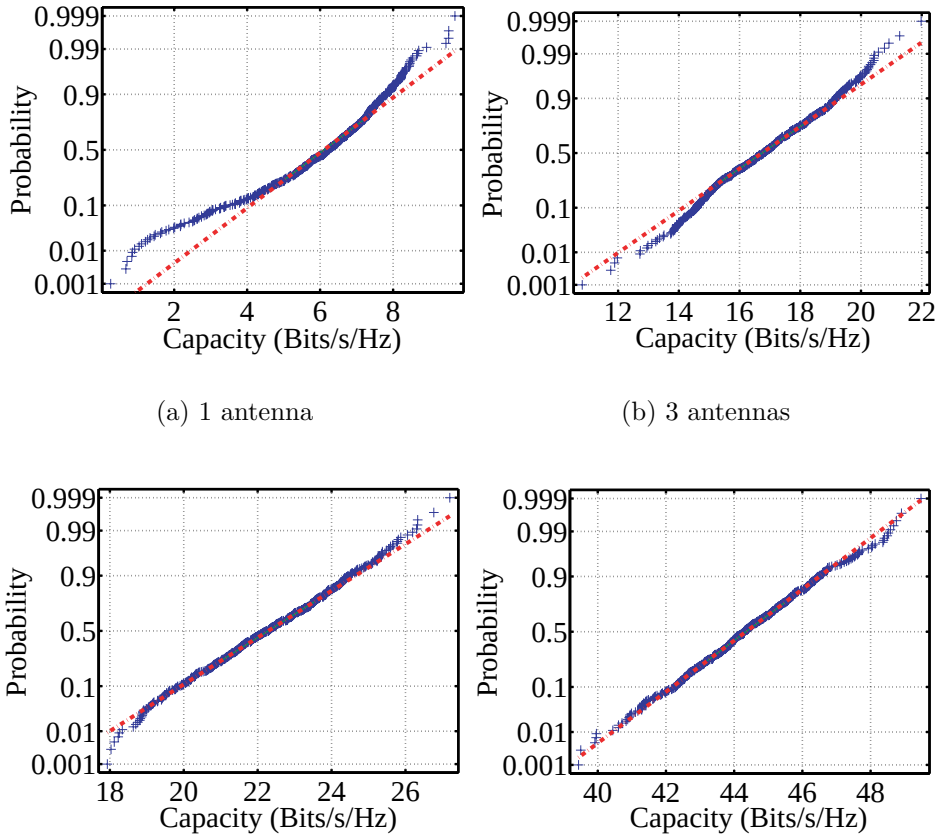

(a) 1 antenna

(b) 3 antennas

(c) 4 antennas

(d) 8 antennas

Figure 6: The normal probability plots of the capacities for 1, 3, 4, and 8 antenna configurations.

used. In these graphs, the vertical axis is distorted in such a way that the CDF for a normal random variable appears as a straight line. The closer the samples are to the dashed line, the closer is the capacity distribution to Gaussian. The plots in Figure 6 show that as the number of antennas increases, the capacity distribution becomes more normal.

For four or more antennas at each node, the plot is linear, indicating that the capacity can be modelled by a normal distribution. More recent studies have verified this surprising result [27, 61].

With this result, simply the first and second order statistics are sufficient to characterize the capacity. An expression for the mean was derived in [70]. The variance

is derived in [61].

The upper bound in 23 is approximated by the Gaussian random variable [27] with mean

$$\mu_{C_{UB}} = K \log_2 \left(1 + \frac{P_T N}{K}\right) - \frac{KN}{M \ln(2)} \left(\frac{P_T}{2K + 2P_T N}\right)^2, \tag{26}$$

and standard deviation

$$\sigma_{C_{UB}} = \sqrt{\frac{N}{M}} \frac{P_T}{\ln(2)\,(1 + P_T N/K)}. \tag{27}$$

This approximation of the MIMO channel capacity demonstrates the dependence of the capacity to the link parameters such as power, number of transmit and receive antennas, and number of streams.

2.6.5 Closed-Loop Capacity and Interference

The problem of deriving the statistics of the capacity becomes even more complicated for CL-MIMO links, or in the presence of interference. Studies of the statistics of the whitened channel mode gains exist only for the case when the receivers are overloaded with interference streams. The authors of [39] follow the results of [40] to derive the distribution of the largest channel mode gain when there are more interference streams than the DOFs at the receiver. However, as we will show in Chapter 4, the performance of a MIMO link with an overloaded receiver is very low with linear processing. Thus, we try to avoid the receiver-overload condition.

2.7 Channel Tracking

Both OL- and CL-MIMO links require perfect knowledge of the channel matrix at the receiver for coherent detection. In CL-MIMO, this information is also needed at the transmitter. The time needed for training and the fading rate of the channel are the two main parameters that determine if the closed-loop operation is feasible.

While noncoherent techniques have been proposed [36], high data rates with low error probabilities are achieved when the wireless channel response is known.

Training-based estimation of flat fading MIMO channels has been studied in [32, 48,64,65]. Assuming that the training is done over L_t symbols, we define the matrices $\mathbf{X}$ and $\mathbf{Y}$ in terms of the transmitted and received sets of vectors as

$$\mathbf{X} = [\mathbf{x}_1 \mathbf{x}_2 \dots \mathbf{x}_{L_t}]$$

$$\mathbf{Y} = [\mathbf{y}_1 \mathbf{y}_2 \dots \mathbf{y}_{L_t}] .$$

Note that $\mathbf{x}_t$ represents the vector of training symbols transmitted at time t. The (unbiased) maximum likelihood (ML) and the linear minimum mean-square-error (MMSE) estimates of the channel matrix are given in [32] as

$$\hat{\mathbf{H}} = \sqrt{\frac{M}{P_T}} \mathbf{Y}\mathbf{X}' \left(\mathbf{X}\mathbf{X}'\right)^{-1} \tag{28}$$

and

$$\hat{\mathbf{H}} = \sqrt{\frac{M}{P_T}} \mathbf{Y}\mathbf{X}' \left(\frac{M}{P_T}\mathbf{I}_M + \mathbf{X}\mathbf{X}'\right)^{-1} . \tag{29}$$

It is shown in [48] that the optimal training signals are orthogonal with respect to time among the transmit antennas, and have equal energy across the transmit antennas. The minimum training interval required for a meaningful channel estimate is equal to the number of transmit antennas, M, and not dependent on the number of receive antennas. Moreover, for the ML estimate, the estimation error for each coefficient of the channel matrix is independent, and distributed as $\widetilde{N}\left(0, \frac{M}{P_T L_t}\right)$.

The length of the training sequence affects the capacity. Although the performance of the estimation improves with longer training, the time left for data transmission decreases. Hassibi *et al.* propose varying the transmit power during training and data transmission intervals [32]. At high SNR, or when the transmission power during training is allowed to be more than the data transmission phase, the optimal training length is shown to be equal to the minimum possible, or M. However, at low SNR, if the transmit power is fixed, the optimal training interval is longer.

Sun *et al.* show in [65] that training-based estimation and linear interpolation of the channel coefficients over time gives reasonable performances. Kalman estimation of MIMO channels is studied in [11], while blind identification methods for MIMO channels are proposed in [46, 66].

2.8 CSI at the Transmitter

MIMO systems with closed-loop operation require CSI at the transmitter as well as the receiver. When CSI is available at the transmitter, spatial filtering can be used at both ends of the link based on the SVD of the channel matrix, as explained in Section 2.4.2.

With TDD operation and under additive white Gaussian noise (AWGN) the channel symmetry property can be exploited to obtain the CSI at the transmitter. If the channel is fairly static, the transmitter can simply use the CSI obtained from a previous burst from the receiver. However, it is shown in [43] that under TDD operation without a feedback channel, the requires CSI update rate is higher than with feedback.

For frequency-division-duplex (FDD) systems with severe multipath environments with large Doppler, angle, and delay spreads, it is argued in [54] that using the spatial covariance of the reverse-link signal improves the network performance.

The channel symmetry approach of TDD operation is no longer optimal in the presence of cochannel interference (CCI). The CSI needed at the transmitter is the whitened channel matrix rather than just the channel matrix, and the whitened channel depends on the interference sensed at the receiver. One node cannot know the interference sensed at another node without some signaling of that information.

Therefore, we assume that the transmitter knows the channel because of explicit feedback.

2.9 OL-MIMO Architectures

In an independent fading environment and for high SNR, OL- and CL-MIMO approaches yield nearly equal capacities [58]. This result and the network overhead required to provide CSI to a transmitter have led to OL-MIMO receiving a great amount of attention in the literature [14, 24, 25, 31, 34, 35].

The original Bell Laboratories Layered Space-Time (BLAST) architecture proposed in [24] is one such approach. It is referred to as diagonal or D-BLAST since it employs a diagonally layered coding structure. The code blocks are dispersed across diagonals in space-time. Through this complicated 2-D coding algorithm the performance of D-BLAST approaches the open-loop capacity.

In the simplified vertical scheme (V-BLAST) [31], every antenna radiates an independently encoded equal-rate data stream. This kind of architecture requires vector (1-D) coding-decoding complexity and overhead, and the resulting capacities are lower. The V-BLAST receiver extracts the streams using ordered successive interference cancellation in coordination with a zero-forcing (ZF) or MMSE filter.

If no channel information is available at the transmitter, each transmitter antenna must use equal power and rate, and the achievable data rate for each transmitted stream is limited by the stream with the least favorable channel. Therefore, depending on the variation in the channel coefficients that each transmit antenna sees, the channel may not support noticeably high data rates with OL-MIMO approaches. V-BLAST can attain 50% of the open-loop capacity [14].

More recent research on BLAST schemes such as [12] and [14] propose to use limited feedback to adjust the rate of each transmitted data stream. A method of power adaptation is also proposed in [14] to better utilize the channel, while keeping the transmitted streams independent. It is shown in [35] that the Demmel condition number of a channel matrix, which is the ratio of the Frobenius norm of the matrix over its minimum singular value, can be used to determine a MIMO channel's

suitability for spatial multiplexing versus transmit diversity.

2.10 CL-MIMO

The highest theoretical MIMO link capacities are obtained using CL-MIMO links. In CL-MIMO, both the transmitter and the receiver know the channel, and can adapt to the spatial characteristics of the channel. The output of each transmit antenna is a linear combination of the multiplexed signals.

CL-MIMO has higher spectral efficiency than OL-MIMO especially in the presence of interference [12, 18, 19], or in correlated fading [59]. If MIMO becomes common in wireless networks, then it will certainly operate in interference-limited environments, where the channel-feedback overhead and the adaptive implementation may become worthwhile.

2.11 Joint Optimization of Cochannel Links

Many studies on MIMO systems consider a single point-to-point link without co-channel interference [14, 24, 25, 31, 50, 53, 70]. We are aware of only one study that briefly discusses the operation of sets of co-channel MIMO links that interfere with each other [23]. This study suggests neglecting the spatial characteristics of interference when determining the link parameters. Equivalently, the interference is assumed to be white. With this simplification, the parameters are calculated with no iterations. However, we believe not only that the interference is actually non-white [44, 62], but also that the non-whiteness figures prominently in joint optimization. Therefore, the link parameters found with this assumption are not optimal. Our simulations have shown that the performance with this assumption can be even worse than the capacities of OL-MIMO links. The importance of joint optimization and stream control will be shown in the following chapters.

The effect of the number of transmitted data and interference streams on MIMO

link performance is investigated in [8]. The results of this study suggest using limited number of streams. However, joint link optimization is not considered in this study.

There are some studies that have considered joint link optimization in cellular systems, where only the base-station has an array antenna. Uplink is considered in [22] and downlink is considered in [26]. Iterative methods are used to determine optimal power control and weight adaptation in these studies. Control over the spatial domain is limited to only one end of the link in these link sets.

Joint transmit and receive beamforming is studied in [13]. However, each link transmits a single stream; thus, the objective and the method of the algorithm given in this study is also different from our problem for the following reasons:

- Beamforming for single-input single-output (SISO) links are considered in [13], which simplifies the metrics used to SIRs instead of link capacities in our MIMO optimization problem.

- The objective of [13] is to optimize the antenna weights and transmit powers to achieve a certain SIRs for each link, whereas in our problem with co-channel MIMO links capacity and transmit power are distributed to each link, as well as to each stream of a link.

- The concept of *virtual uplink* is used to determine the downlink transmit weights in [13]. However, in our situation, the interference for each direction of data flow is different, thus the reciprocal channel assumption is not valid.

In the next two chapters, we consider joint optimization of cochannel CL-MIMO links. The two iterative algorithms given in the next chapter and the stream control algorithm developed in Chapter 4 aim to maximize the network throughput and control the capacities of the interfering links.

CHAPTER 3

JOINT OPTIMIZATION OF INTERFERING MIMO LINKS

In this chapter we consider joint optimization of power and array weights for a set of interfering CL-MIMO links. We assume a stationary, flat Rayleigh fading environment, and that both the receiver and the transmitter nodes have perfect knowledge of the (whitened) channel.

We want to determine methods of controlling the relative capacities of the links and obtain optimal transmission strategies corresponding to different QoS requirements and network topologies. The set of parameters to be determined for each link includes the total transmit power, the number of parallel streams transmitted, the transmit and receive weight vectors, and power allocated to each stream.

Combinations of constraints are possible for this problem, such as desired capacities, total transmit powers, and number of parallel streams transmitted by each link. We present two distributed iterative methods that jointly optimize the power and array weights for the co-channel CL-MIMO links. The first (power-controlled) method is used to determine the array weights and link capacities based on predetermined total transmit powers, while the second (capacity-controlled) method gives array weights and total transmit powers necessary to meet target capacity constraints.

Shown in Figure 7 are two simple networks with two and three links, respectively, that are considered in our simulations. The links are shown by the solid arrows. The dashed arrows show the sources of interference. Each node has an array-antenna with four elements spaced sufficiently far apart to have independent fading. The link

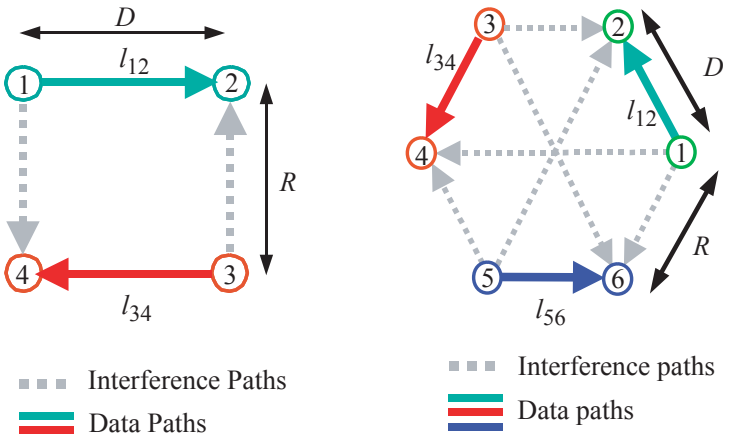

(a) Two-link network. (b) Three-link network.

Figure 7: Two simple networks considered in the simulations.

between nodes i and j is denoted by l_{ij}. The channel gain depends on the distance between the nodes, assuming a path-loss exponent of 3. Therefore, as R/D increases, the SIR decreases.

In the next section we establish the mutual dependence of interfering link parameters due to transmit beamforming and power allocation. A discussion of the central solution of our optimization problem follows. In the next two sections we present two joint link adaptation methods for co-channel CL-MIMO links.

3.1 Mutual Dependence of Interfering Link Parameters

In a network with multiple interfering links, the interference correlation matrix seen by each receiver array varies with the transmitter correlation matrices of the interfering nodes. The whitened channel matrix, $\widetilde{\mathbf{H}}$, for a given link is a function of the interference, $\mathbf{R}$. The transmission strategy, in turn, is dependent on the whitened channel matrix.

Thus, a change in the power allocation matrix of one link induces a change in

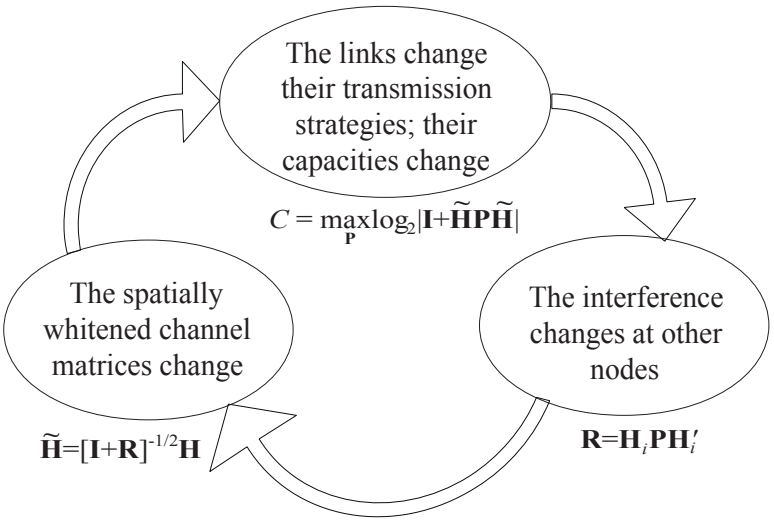

Figure 8: The optimum transmission strategies and the capacities of interfering MIMO links are mutually dependent.

the optimum power allocation matrix of the other co-channel links. Therefore, the optimum transmission strategies and the capacities of interfering MIMO links are mutually dependent. This is summarized in Figure (8).

As a result, the optimum transmit weights and powers of interfering CL-MIMO links cannot be calculated independently at each link. Iterative methods are used. Studies considering transmit beamforming for single-stream links [13, 22] have also used iterative methods.

3.2 Central Solution

Global numerical optimization of all antenna weights to optimize network throughput is computationally prohibitive even if the channel gains between all pairs of nodes are centrally gathered.

The parameters to be optimized are the elements of the complex transmit-signal correlation matrix[1] for each link. The rank of this matrix gives the number of channel modes used, and the eigenvectors give the transmit weight vectors for each

[1]See Section 2.4.2 for definition.

link. The receive weight vectors are determined from the channel and the transmit-signal correlation matrices. The number of parameters to be determined increases with the square of the antenna-array size, and linearly with the number of links.

As shown in the previous section, the matrices for different links are jointly dependent. Moreover, the quantity to be optimized, the total network throughput, is not a convex function, nor it is a linear function of the control variables.

Numerical search methods are not feasible even with few links and small-size arrays. Well-known optimization methods that make approximations of the Hessian function such as sequential quadratic programming [28, 56] do not yield successful solutions with high probability, and the solutions are local.

The simplicity and the fast convergence of the distributed iterative algorithms presented in the next two sections make them attractive even for centrally controlled network systems.

3.3 Power-Controlled Method

A distributed iterative method is used to determine suboptimal transmitter correlation matrices and receiver transformations in a network with interfering CL-MIMO links for given total transmitter powers [17]. These matrices and transformations converge to final values within few iterations.

Each set of transmit powers give a different set of capacities for each link. Therefore, transmit power can be used as the control parameter to allocate capacities as desired to each of the interfering links.

3.3.1 Algorithm

At each iteration, every transmitter-receiver pair optimizes its link capacity for the measured interference at the receiver, and its respective given total transmitted power. Each link's transmission strategy is determined according to the water-filling solution given in (11) for the current spatially whitened channel.

Note that with this iterative algorithm, the transmission strategies for a given link are found based only on the channel gains for that link and the interference correlation matrix observed at the receiver array for that link. The knowledge of the channel gains between other transmitter-receiver pairs is not necessary.

3.3.2 Convergence

The stopping criterion for the iterative method is that all link capacities must change less than 0.01 bps/Hz. If convergence is not reached within 50 iterations for a trial the simulations are stopped.

Figures 9 and 10 demonstrate the convergence characteristics of the power-controlled algorithm for our sample networks with equal node distances and 4 antenna elements at each node. The noise-normalized total transmit power is 20dB for each link. The starting point represents OL-MIMO performance. Figure 9(a) shows the convergence of the capacities of the two links of the two-link network for one channel trial. Figure 9(b) shows the variation in the total throughput with the iterations for four different channel trials. The most improvement takes place in the first two-three iterations.

Figure 10 shows the histograms of the number of iterations needed for convergence for both two- and three-link networks. For the two-link network, the median of the number of iterations is 6, converged values are obtained within 20 iterations for 96% of the trials, and only 1% of the trials did not converge within 50 iterations. For the three-link network, the median of the number of iterations is 9, 95% of the trials have converged within 20 iterations, and the rate of the trials that did not converge within 50 iterations is 2%.

The few trials in which the capacities did not converge within 50 iterations are the cases that have oscillatory behavior between two states, because the links fight over a stream in this trial. Figure 11 shows the change in the capacities of the two

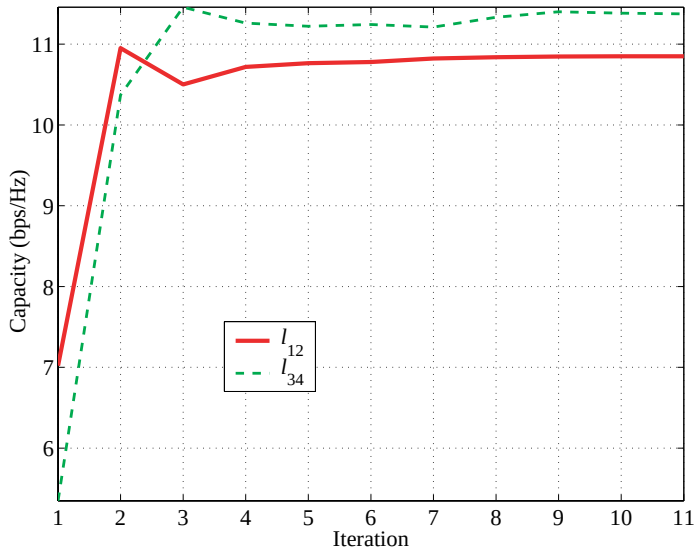

(a) Convergence of the capacities of the two links for one channel trial.

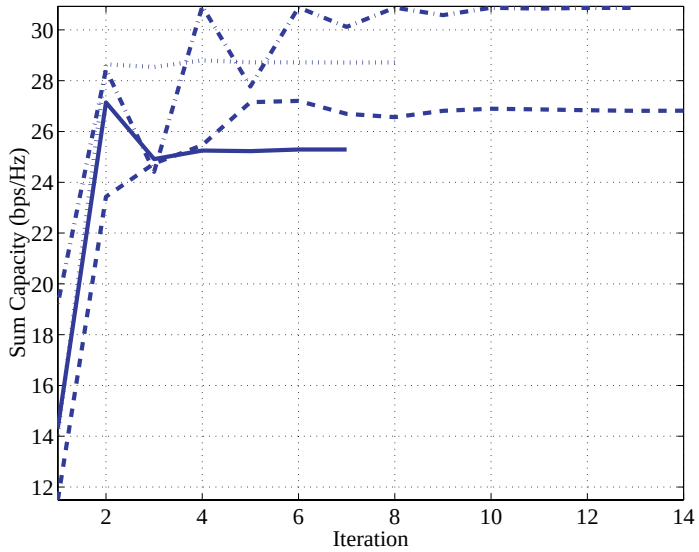

(b) Time variation of the throughput (the sum capacity of the two links) for four channel trials.

Figure 9: Convergence characteristics of the capacity-controlled joint link adaptation method for the two-link network.

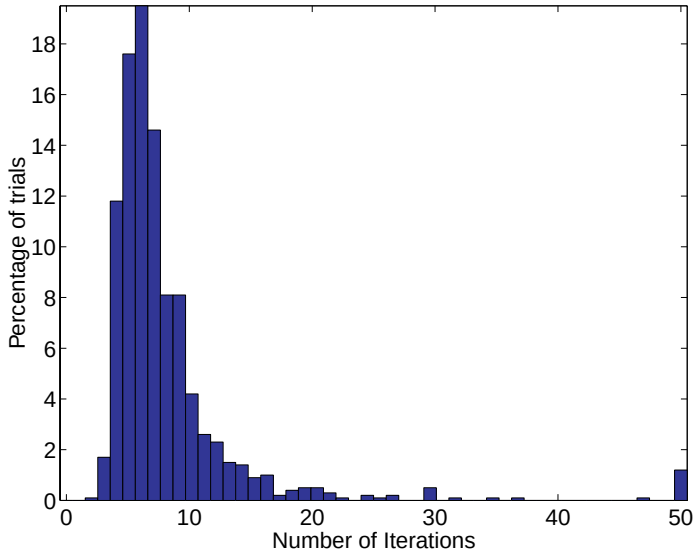

(a) Two-link network.

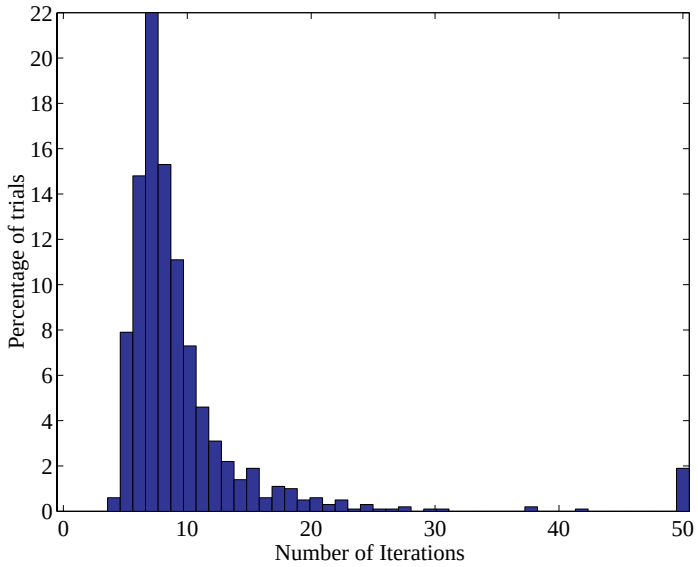

(b) Three-link network.

Figure 10: Histograms of the number of iterations needed for convergence of the power-controlled iterative algorithm.

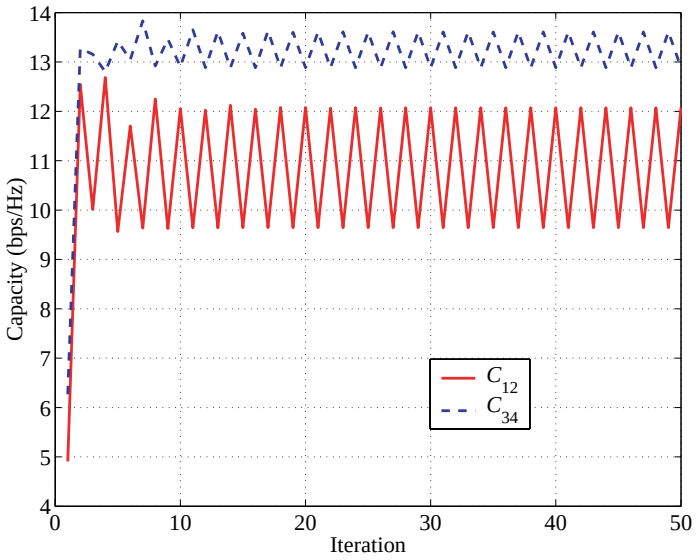

Figure 11: A trial with oscillatory behavior between two states.

links for one such trial.

3.3.3 Results

For the three-link network with equal distances, an illustration of the dependence of the link capacities on total transmitted powers is given in Figure 12. The figure shows the 90% confidence intervals of the capacities of the three links found by the iterative method explained above for different total powers transmitted. Two different viewpoints are shown. There are two surfaces for each link, showing the upper and lower interval boundaries. For each set of channel realizations, the capacities are found iteratively, for 4000 channel trials. The two horizontal axes represent the total powers transmitted from nodes 3 and 5, respectively, which vary from 0 to 20dB. The power of node 1 is held constant at 20dB. The vertical axis is the capacity in bits/s/Hz. For each set of powers the capacities found are different. The surfaces are not symmetric with respect to the line of equal powers for nodes 3 and 5. This is because the transmitter in l_{12} makes stronger interference on the receiver of l_{56} than it does on the receiver of l_{34} because the distances are not the same. However, there are some points of symmetry; for example, the mean capacity of l_{34} at the

coordinates $(P_3, P_5) = (20, 0)$dB equals the mean capacity of l_{12} at the coordinates $(P_3, P_5) = (0, 20)$dB, because of the symmetry of the hexagon. The confidence interval widths are small, ranging from 2 to 5 bits/s/Hz. The interval width is larger when there is more interference.

Figure 13 shows the cumulative distribution functions (CDFs) of the capacities obtained from the simulations when the links use equal power. The curve in the middle corresponds to the capacity of one link when there is no interference from the transmitters of the other links. This CDF is the same for all three links, because all links have the same transmitter-receiver distance. The curve on the left is the CDF of one link's capacity when all three transmitters are on, with a noise-normalized-power of 20dB. Because of the symmetry of the hexagon, this CDF is also the same for all links.

The curve on the right is the CDF of the total capacity when the three links are active at the same time. This data is three times the data for the curve on the left. The difference between the right and the middle curves is about 3 bits/s/Hz at the median; this shows that, for our equally spaced three-link network, approximately a 12.4% capacity gain is obtained when the links are allowed to operate simultaneously, as opposed to a system where nodes take turns to transmit.

When co-channel links operate simultaneously, all nodes transmit continuously, and each link has a lower capacity than it would have in the absence of interference. However, in a TDMA network the nodes use transmit power only during their scheduled time slots. Although there is a gain in the total capacity utilized in this analysis, more power is transmitted in the network. In an equal-energy setting the throughput with interfering links would be less than what is shown in this section, because the transmit power of each link would have to be lower.

On the other hand, it will be shown in the next chapter that better performances are possible through an extension of the algorithm; by stream control. In Chapter 5

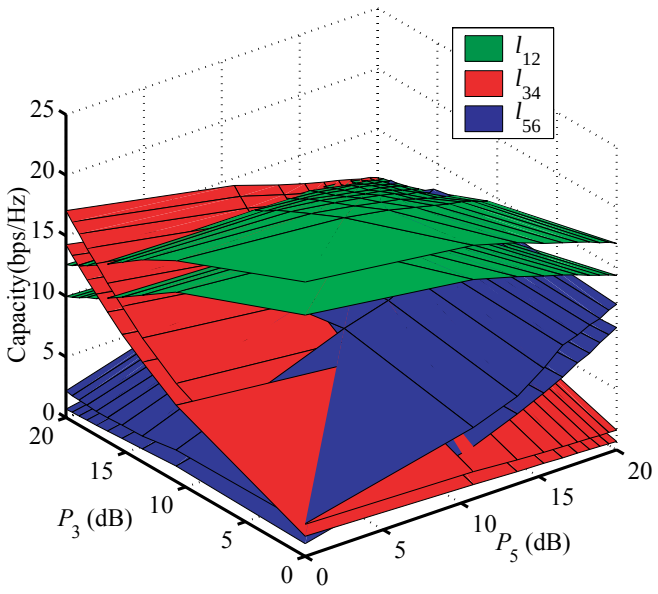

(a) Front view.

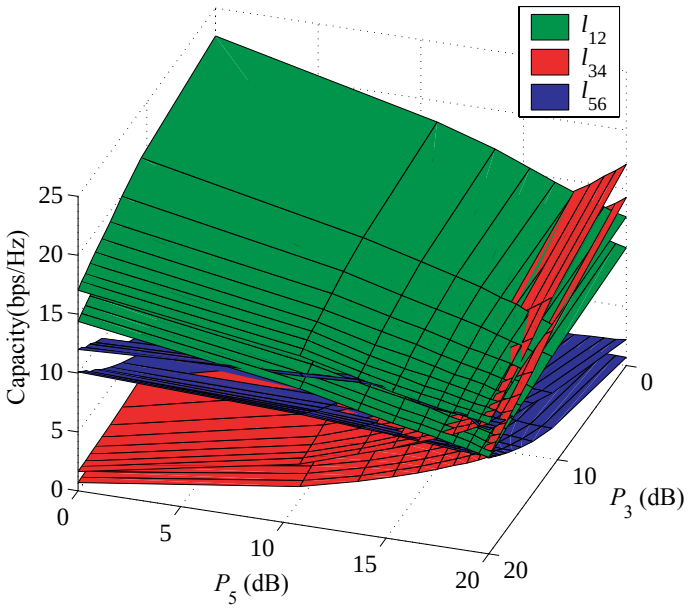

(b) Rear view.

Figure 12: Ninety-percent confidence intervals for the capacities of the links as a function of the noise-normalized total transmitted powers.

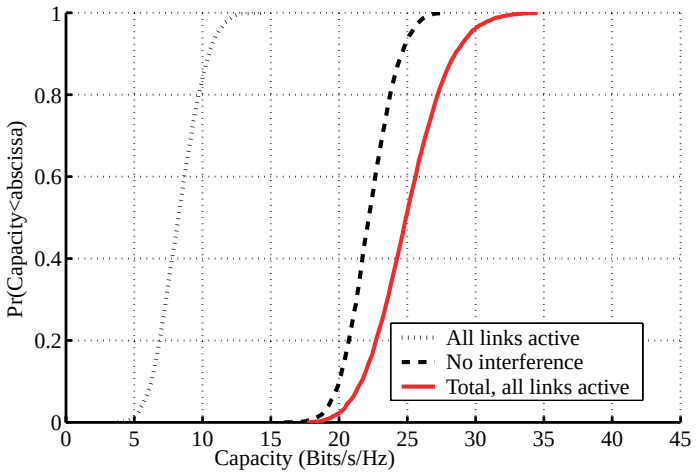

Figure 13: CDFs of the capacities. The curve in the middle is the for one link when there is no interference, the curve on the left shows the capacity of one link when all three transmitters are on (all with 20dB transmit power), the one on the right is the total capacity when the three links are active at the same time.

we will give a more detailed comparison of the throughputs with different settings.

In the algorithm we have developed, relative capacities could be controlled by a network genie only after the information in the graph of Figure 12 has been captured. The genie simply tells the different nodes what total powers they are allowed to use and then they use the iterative distributed algorithm to optimize their respective link capacities.

This algorithm is useful if we want to get the maximum possible capacity for each link with given transmit powers. Next, we explore a different approach that can be more practical in some cases.

3.4 Capacity-Controlled Method

Whereas in the previous method we aimed for the highest link capacities given the total transmit powers, we now assume that the desired capacities are given for the interfering MIMO links and want to determine optimal transmission strategies and the required transmit powers. Therefore, the control parameters to allocate capacities to each of the interfering links are the desired capacities.

Another major difference of this algorithm [18] from the power-controlled method is that the transmitter node of a link can also make use of the knowledge of the channel with neighboring receivers, as well as the one that it aims to communicate with. Therefore, if more information is available about the channels, it can be utilized to speed up the convergence process.

With this method, the transmitter node of one link tries to minimize a measure of interference it causes at the receiver of another while aiming for the link's target capacity. Thus, transmitter power of a link is distributed to the channel modes in a way to least degrade the other links. This method also tends to minimize the total transmitter power required to achieve the target capacity.

3.4.1 Algorithm

As with the previous method, we use an iterative algorithm to solve our optimization problem. At each iteration, every transmitter-receiver pair optimizes its link capacity for the measured channel and interference conditions. This type of iterative algorithm has been proven to converge for mobile users with omnidirectional antennas and cellular base stations with MEAs [26].

Rather than simply trying to minimize a transmitter's total power, we can take advantage of our assumption that each transmitter knows its MIMO channels with its neighbors and be more selective by minimizing the interference power it makes on its neighbor. This can be accomplished by minimizing the trace of the autocorrelation matrix of the interference sensed at the victim receiver.

For illustration we look at the four-node network of Figure 7(a). Suppose we would like to get the maximum capacity for l_{12}, and set a target capacity, C_T, for the other link. In other words, l_{12} maximizes its capacity using the water-filling based method given in the previous subsection for its fixed total noise-normalized transmit power, while l_{34} uses the interference-minimizing power allocation method to achieve

its target capacity. The problem optimization to be solved to obtain the transmission strategy at node 3 can be stated as

$$\min_{\mathbf{P}_{34}} trace\left[\mathbf{R}_{32}\right] \quad \text{s. t.} \quad \begin{cases} C_{34} = C_T \\ trace\left[\mathbf{P}_3\right] \leq P_{max} \end{cases} \tag{30}$$

$\mathbf{R}_{32} = \mathbf{H}_{32}\mathbf{P}_{34}\mathbf{H}'_{32}$ is the correlation matrix of the interference caused by node 3 on 2, and P_{max} is the maximum noise-normalized transmit power. As in the power-controlled algorithm, the eigenvectors of the power allocation matrix should be aligned with the right singular vectors of the whitened channel matrix, $\mathbf{H}_{34}$. Therefore, with

$$\widetilde{\mathbf{H}}_{34} = \left[\mathbf{I} + \mathbf{R}_{14}\right]^{-1/2}\mathbf{H}_{34} = \widetilde{\mathbf{U}}_{34}\widetilde{\mathbf{S}}_{34}\widetilde{\mathbf{V}}'_{34}, \tag{31}$$

the power allocation matrix should be of the form

$$\mathbf{P}_3 = \widetilde{\mathbf{V}}_{34}\mathbf{\Sigma}_{34}\widetilde{\mathbf{V}}'_{34}, \tag{32}$$

where $\mathbf{S}_{34}$ and $\mathbf{\Sigma}_{34}$ are diagonal. We would like to determine the power to be allocated to each mode of l_{34}, $\alpha_{34,k}$, which are the nonzero elements of $\mathbf{\Sigma}_{34}$. The eigenvalues of $\widetilde{\mathbf{H}}_{34}\widetilde{\mathbf{H}}'_{34}$ are represented as $\widetilde{\lambda}_{34,k}$. The trace of the interference correlation matrix can be written in terms of $\alpha_{34,k}$ as follows:

$$\begin{aligned} trace\left[\mathbf{R}_{32}\right] &= trace\left[\mathbf{H}_{32}\widetilde{\mathbf{V}}_{34}\mathbf{\Sigma}_{34}\widetilde{\mathbf{V}}'_{34}\mathbf{H}'_{32}\right] && (33)\\ &= trace\left[\widetilde{\mathbf{V}}'_{34}\mathbf{H}'_{32}\mathbf{H}_{32}\widetilde{\mathbf{V}}_{34}\mathbf{\Sigma}_{34}\right] && (34)\\ &= trace\left[\mathbf{\Phi}\mathbf{\Sigma}_{34}\right] && (35)\\ &= \sum_{k=1}^{K}\phi_k\alpha_{34,k}, && (36) \end{aligned}$$

where $\mathbf{\Phi} = \widetilde{\mathbf{V}}'_{34}\mathbf{H}'_{32}\mathbf{H}_{32}\widetilde{\mathbf{V}}_{34}$, ϕ_k is the k^{th} diagonal element of $\mathbf{\Phi}$, and we have used $trace\left[\mathbf{AB}\right] = trace\left[\mathbf{BA}\right]$. Therefore, our cost function at node 3 reduces to

$$\min_{\alpha_{34,k}} \sum_{k=1}^{K}\phi_k\alpha_{34,k} \quad \text{s. t.} \quad \begin{cases} \sum\limits_{k=1}^{K}\log_2(1+\widetilde{\lambda}_{34,k}\alpha_{34,k}) = C_T \\ \sum\limits_{k=1}^{K}\alpha_{34,k} \leq P_{max} \end{cases} \tag{37}$$

Note that when multiple unintended receivers are present, ϕ_k is replaced by a (possibly weighted) sum of terms, each corresponding to the interference effect due to the k^{th} stream at an unintended receiver.

The solution is

$$\alpha_{34,k} = \left[\frac{\mu}{\phi_k + \nu} - \frac{1}{\widetilde{\lambda}_{34,k}} \right]^+, \tag{38}$$

where μ and ν are constants chosen such that the constraints in (37) are satisfied.

Notice the similarity of this expression to the water-filling solution in (11).Whereas we had a fixed maximum level, μ, for all power coefficients of the channel modes in (11), with this solution, we have different maximum levels for each $\alpha_{34,k}$. Each of these levels depends on the strength of the interference that the corresponding channel mode causes.

We could be even more selective in the penalty by somehow weighting the interference according to the impact that it has on the victim link. This can be done by replacing the metric minimized above by its projection onto the victim link's channel.

On the other hand, if a transmitting node does not have the knowledge of the channel with the neighboring receivers, it can simply minimize its transmit power instead of the trace of the induced interference correlation matrix.

3.4.2 Convergence

Figure 10 shows the histogram of the number of iterations needed for convergence for the two-link network, when link l_{34} uses the capacity-controlled method. Again, the node distances are equal ($R = D$) and each node has 4 antenna elements. The noise-normalized total transmit power of l_{12} is 20dB, and the target capacity of l_{34} is 5bps/Hz.

The stopping criterion is the same as that used with the power-controlled method. All link capacities must change less than 0.01 bps/Hz. If convergence is not reached within 50 iterations for a trial the simulations are stopped.

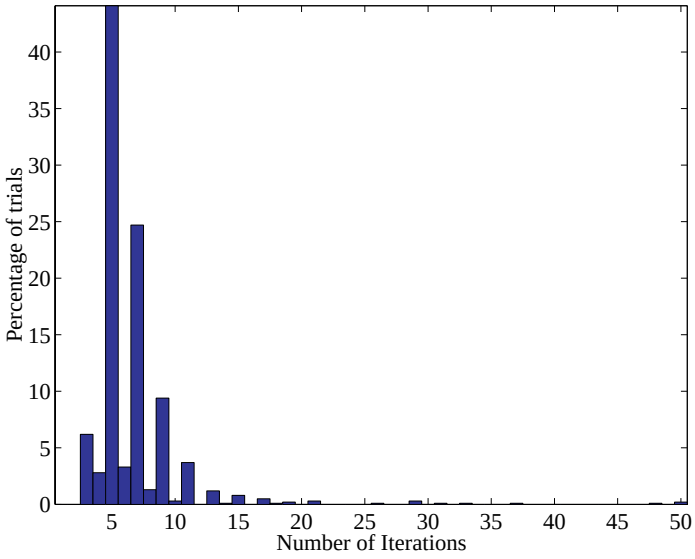

Figure 14: Histogram of the number of iterations needed for convergence of the capacity-controlled iterative algorithm.

The median of the number of iterations is 5, converged values are obtained within 20 iterations for 99% of the trials, and only 0.2% of the trials did not converge within 50 iterations.

Capacity-controlled method converges with fewer iterations than the power-controlled method. This is because the transmitting nodes are assumed to have more knowledge (CSI through the interference paths). However, when the desired capacities are large (i.e. when they are hardly realizable with the maximum transmit power constraints at each link), the computation required for each iteration at each link increases. The power-controlled method requires less computing per iteration, since only one lagrangian is to be determined.

3.4.3 Results

Figure 15(a) shows the capacities of the two links as the target capacity of l_{34} is varied. The top two constant lines show the capacities of the two links for this channel trial in the absence of any interference with 20dB noise-normalized total transmit powers.

The two constant lines below show the capacities of the links found by the power-controlled algorithm for equal transmitter powers when both links are active. The line with the constant positive slope is the target capacity of l_{34}. The decreasing curve is the capacity of l_{12}. A maximum transmit power of 20dB is used for l_{34}.

Figure 15(b) shows the total transmit power required to achieve the desired target capacity. As the target capacity of l_{34} is increased, the transmit power required at node 3 goes up. Consequently, l_{34} is degraded by more powerful interference streams (by a larger number of streams, in some cases), and thus, its capacity decreases.

For equal transmit powers, the link capacities found with both methods are equal. This can be observed from the fact that the capacities calculated by the capacity-controlled method converge to the values found by the power-controlled method as the target capacity increases in Figure 15(a). At the point where the capacities curves corresponding to the two different methods intersect, the transmit power for l_{34} converges to 20dB.

Although it was illustrated on only l_{34}, this method can be employed at all links in a network to find optimal transmission strategies and transmitter powers when the desired set of capacities is given.

As with the power-controlled method, it will be shown in the next chapter that better performances are possible by an extension of the algorithm. Namely, controlling the number of streams for each link to limit the number of interfering streams in the network increases the overall throughput for both methods.

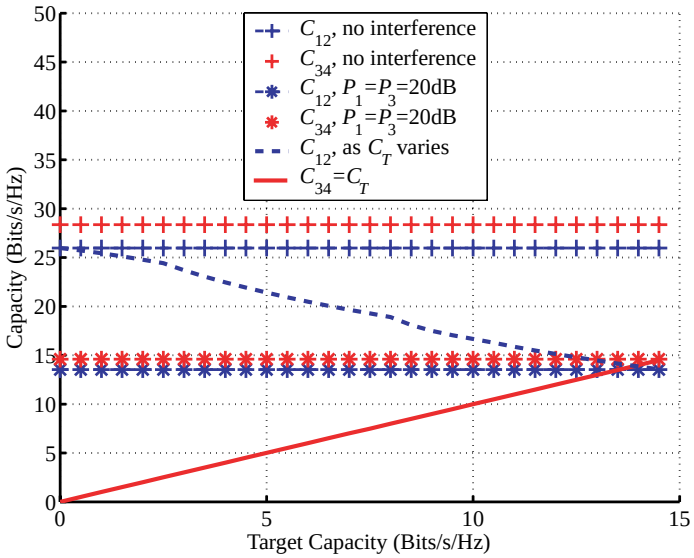

(a) Link capacities vs. target capacity of node 3.

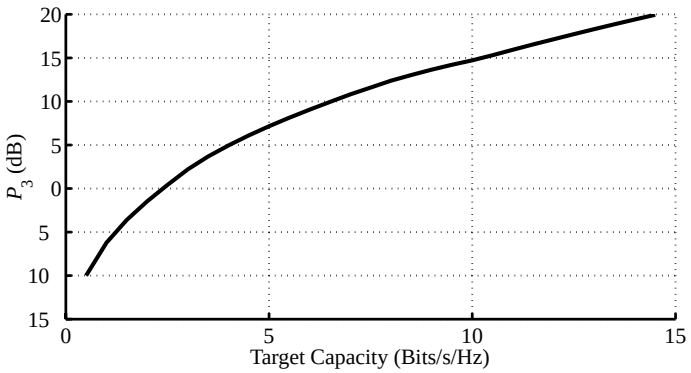

(b) Required total transmit power vs. target capacity of node 3.

Figure 15: Dependence of the link capacities and required transmit power of node 3 as target capacity of node 3 is varied, for an example trial.

CHAPTER 4

STREAM CONTROL

Both methods introduced in the previous chapter are distributed; each link determines its own transmission strategy based on the local channel conditions. The cost functions considered are not based on the total network throughput, but on the capacities of the individual links. Although the two iterative methods allow multiple co-channel CL-MIMO links to operate simultaneously, they do not always maximize the total network throughput. A link's performance is not only degraded by the power of the interference received, but also, and more importantly, by the number of interfering streams.

In this chapter, we show that controlling the number of transmitted streams in each link in the network enhances the performance of interfering MIMO links. A distributed algorithm which exploits CSI at the transmitter is presented for determining the maximum number of independent data streams for each transmitting node in a network of interfering MIMO links.

4.1 Number of Streams and Receiver Overload

The key to achieving a large capacity for a single MIMO link is to partition a single high SNR channel into many lower SNR subchannels. In OL-MIMO links, partitioning is over the transmit antennas and in CL-MIMO links, it is over channel modes. However, when multiple interfering links are considered, partitioning into sub-channels creates more uncorrelated interference streams.

In CL-MIMO links, the water-filling solution does not necessarily excite all of the possible channel modes. Therefore, one might think that when water-filling is done

iteratively for interfering MIMO links, the solution at convergence would automatically find the best number of streams to optimize network throughput. However, this is not always the case [18, 19]. We attribute this to the fact that in the distributed algorithms introduced in the previous section, all links are trying to maximize their own capacities at the same time; network throughput is not the cost function being optimized.

For independent flat-Rayleigh fading wireless systems, the data streams can be resolved effectively by linear processing if the number of data and interference streams is less than or equal to the number of receive antennas [9,76]. However, in some cases the distributed link adaptation algorithms overload the receivers with more streams than the available DOFs. When the receivers are overloaded, the gain of using an additional stream at one link may be more than offset by the loss at the other links due to the additional interference stream.

As a result, limiting the number of streams transmitted, thus reducing the different sources of interference, may yield better performance [9]. Note that even if the total interference power is constant, an increase in the number of interfering streams reduces the link capacities because of the limitation of DOFs at the receiver nodes.

In OL-MIMO links each transmit antenna radiates an independent stream. Limiting the number of streams would require employing only a subset of the transmit-array elements. Therefore, the size and the gain of the channel matrix $\mathbf{H}$ is reduced.

In CL-MIMO links the streams are transmitted over uncoupled channel modes, or the nonzero eigenvalues of the channel gain matrix, $\mathbf{HH}'$. Limiting the number of streams, in this case, means allocating the transmit power over few strongest channel modes even if equations (11) or (38) would excite more modes. However, all transmit antennas would be utilized. Therefore, there is a significant antenna gain advantage over OL-MIMO links.

The problem of array-subset selection for OL-MIMO links with low-rank channels

and without interference has been studied in [7,30,34]. These studies assume limited feedback of CSI to the transmitter. We focus on distributed stream control for CL-MIMO links as an extension for our joint link adaptation methods.

4.2 Performance With and Without Stream Control

We shall consider the previous two-link topology of Figure 7(a), assuming the noise-normalized total transmit power of each link is set to 20dB, and each node is assumed to have 4 antennas.

Figure 16 shows histograms of the number of streams used by link l_{12} with no stream control and with the globally optimum number of streams. 100 channel trials are generated, and the link parameters are found using the power-controlled method for 20 different values of R/D taken on the logarithmic scale from 0.1 to 250. To get the optimum number of streams power-controlled method is modified to limit the maximum number of streams used by a link. All combinations of allowed number of streams are tried, and the combination with the highest throughput is selected. With the distributed adaptation methods, the links use excessive number of streams without stream control in the region $0.5 < R/D < 3$. For example, when $R/D = 1.786$, l_{12} used 3 streams in 80 channel trials with no stream control, while with optimal stream control it used 3 streams in only 26 trials, and 2 streams in 68 trials. When $R \ll D$, the interference is strong enough that water-filling naturally blocks some of the channel modes. On the other hand, when $R \gg D$, all dimensions can be used despite the incoming interference.

To show the effect of overloading the receivers on the capacity of the links, we consider the two-link network of Figure 7(a) with equal distances between each node ($R/D = 1$) and 4-antenna arrays at each node. We use the power-controlled method to calculate the links' capacities, introducing an additional constraint in the maximum

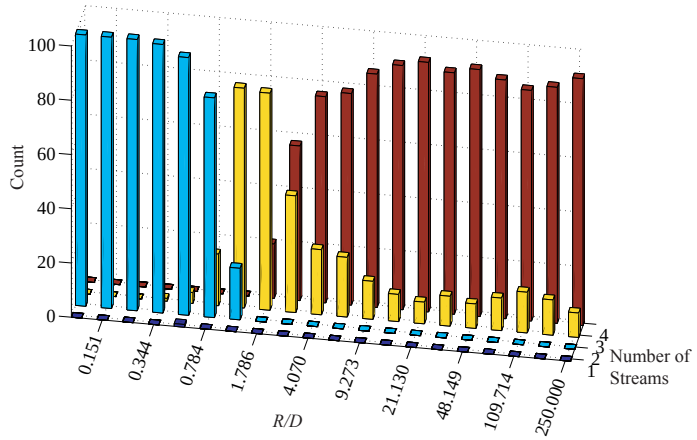

(a) No stream control.

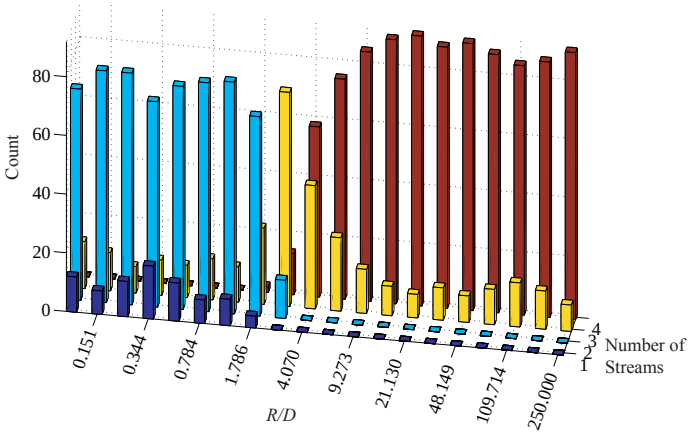

(b) Globally optimum stream control.

Figure 16: Histograms of the number of streams of one link with different CL-MIMO configurations for different R/D values. 20 values of R/D are selected on logarithmic scale from 0.1 to 250.

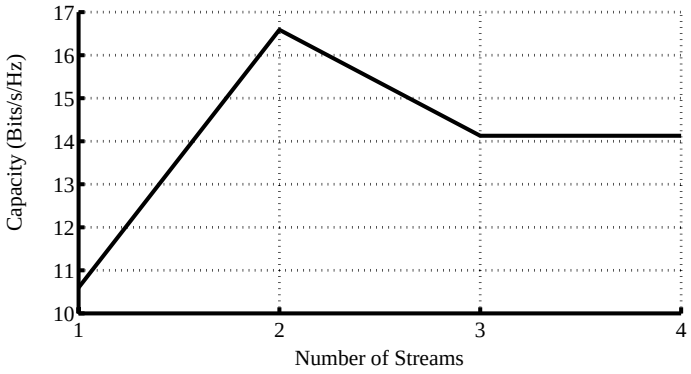

Figure 17: Capacity vs. number of streams used at each link.

number of streams each link can use. Figure 17 shows each link's capacity, averaged over 1000 channel trials, as the number of allowed streams is varied. The total transmit powers of both links are 20dB. The highest capacity is reached when the number of streams for each transmitter is limited to 2. For this case, each link transmits through at most the 2 strongest channel modes. Each receiver receives at most two streams of data and two streams of interference. In accordance with Figure 16(a) for $R/D = 1$, the links use 3 streams in most of the trials with no stream control, therefore, the average capacities for 3 and 4 allowed streams are equal.

Both capacity allocation algorithms perform better with control on the number of channel modes used at each link based on the number of transmitting nodes in the neighborhood. Stream control increases the total network throughput, and reduces the convergence time of the algorithms. In the next section, we propose a distributed algorithm to limit the number of streams for each MIMO link. In the next chapter we analyze the network throughput and demonstrate the performance of our stream control algorithm.

4.3 Stream Control Algorithm

To build a criterion to control the number of streams for the two link network in Figure 7(a), we first rewrite the link capacity in (10) as

$$C_{ij} = \sum_{k=1}^{K} \log_2 \left[\mu_{ij}\lambda_{ij,k}\right]^+ . \tag{39}$$

We look at a special case where all spatial dimensions are filled with data and interference streams, yet node 3 tries to increase its number of streams from L to $L+1$. For instance, assuming that each node has 4 antenna elements, each link could be transmitting 2 streams, and node 3 could try to add a third stream.

4.3.1 Worst-Case Interference

We shall assume that the additional interference stream is spatially aligned with the strongest channel mode of l_{12}. Equivalently, we assume that our strongest channel mode is degraded, and the other modes remain unchanged. This is a worst case interference assumption, as proven in [1], and illustrated in Figure 18 and Table 1.

Figure 18 shows four sets of channel mode gains, with each set corresponding to a certain number, J, of independent interference streams. Each interference stream has the same average power as the desired signal at the receiver. Because each node has 4 antennas, there are four mode gains for each set. For example, the rightmost CDF is for the strongest mode for the $J = 0$, or no interference, case. The next rightmost solid curve is the CDF of the second-strongest mode gain for the $J = 0$ case. The table shows the means values of the gains. The largest $4 - J$ gains of the channel with J interfering streams are greater than the gains, $\widetilde{\lambda}_k, k = 2, \ldots, 4 - J + 1$, of the channel with $J - 1$ interfering streams for all meaningful values of J ($J = 1, 2, 3$). Therefore, our assumption results in a weaker channel than what we actually get.

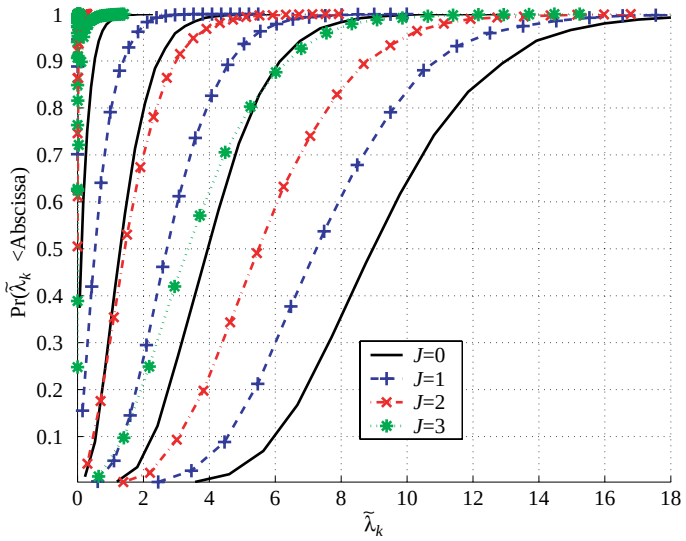

Figure 18: CDFs of the channel mode gains, $\widetilde{\lambda}_k$, of a 4×4 whitened channel that is degraded by different numbers of interference streams.

Table 1: Means of the channel mode gains of a 4×4 MIMO channel degraded by J interfering streams.

	$J = 0$	$J = 1$	$J = 2$	$J = 3$
$\widetilde{\lambda}_1$	9.7732	8.0567	6.2165	4.0279
$\widetilde{\lambda}_2$	4.4431	3.1664	1.8357	*0.0737*
$\widetilde{\lambda}_3$	1.5803	0.8056	*0.0183*	*0.0082*
$\widetilde{\lambda}_4$	0.2496	*0.0033*	*0.0014*	*0.0009*

4.3.2 Algorithm

With the additional interference stream directly degrading the strongest mode, the change in the channel mode gain would be

$$\widetilde{\lambda}_{12,1} \rightarrow \frac{\widetilde{\lambda}_{12,1}}{1+r_{32}}, \tag{40}$$

where r_{32} is the noise-normalized power of the stream at node 2. In this case, transmit power would be reallocated to the modes of l_{12}. The contribution of this mode to the capacity would decrease, while the capacity due to the other modes would increase. Hence, the reduction in the capacity of l_{12}, or ΔC_{12}, would be bounded by

$$\Delta C_{12} \leq \log_2 \left[\frac{\mu_{12}\widetilde{\lambda}_{12,1}}{\mu'_{12}\frac{\widetilde{\lambda}_{12,1}}{1+r_{32}}} \right] < \log_2 \left(1+r_{32}\right). \tag{41}$$

Here, μ_{12} and μ'_{12} are the top *water levels* found by (11) before and after the extra interference stream is excited, respectively, and $\mu_{12} < \mu'_{12}$.

With the additional stream, the increase in the capacity of the link between nodes 3 and 4 is

$$\begin{aligned} \Delta C_{34} &= \sum_{k=1}^{L+1} \log_2 \left[\mu_{34,L+1}\widetilde{\lambda}_{34,k}\right] - \sum_{k=1}^{L} \log_2 \left[\mu_{34,L}\widetilde{\lambda}_{34,k}\right] \\ &= \log_2 \left\{ \frac{\left[\mu_{34,L+1}\right]^{(L+1)}}{\left[\mu_{34,L}\right]^{L}} \widetilde{\lambda}_{34,L+1} \right\}, \end{aligned} \tag{42}$$

where $\mu_{34,L}$ and $\mu_{34,L+1}$ are the top levels with L and $L+1$ modes, respectively.

To assure gain in total throughput we need $\Delta C_{34} > \Delta C_{12}$. Requiring the upper bound given on the right side of (41) to be less than the term on the second line of (42), we get the following condition that assures a positive change in the total network throughput:

$$\alpha_{34,L+1} g_i < \left[\frac{\mu_{34,L+1}}{\mu_{34,L}}\right]^{L} \left(1+\alpha_{34,L+1}\widetilde{\lambda}_{34,L+1}\right) - 1. \tag{43}$$

In this relation, r_{32} has been replaced by $\alpha_{34,L+1}g_i$, where $\alpha_{34,L+1}$ is the power allocated to the channel mode by node 3, and g_i is the corresponding channel gain along the

interference path from node 3 to 2. Note that $\alpha_{34,L+1}\widetilde{\lambda}_{34,L+1}$ is the SNR of the additional stream at node 4, and $\alpha_{34,L+1}g_i$ is the interference-to-noise ration (INR) caused by this stream at node 2.

The largest value g_i can take is largest mode gain, $\lambda_{32,/max}$, of the the channel between nodes 3 and 2. Assuming M and N are the numbers of antenna elements at nodes 2 and 3, respectively, an upper bound on the expected value of $\lambda_{32,\max}$ is given in (21) and in [3] as

$$\lambda_{32,\max} < \frac{(\sqrt{M}+\sqrt{N})^2}{R^n}. \tag{44}$$

Replacing g_i in (43) with the upper bound given in (44) and solving for the interference path length, we get the following condition for allowing node 3 to add another stream:

$$R^n > \frac{\alpha_{34,L+1}(\sqrt{M}+\sqrt{N})^2}{\frac{\left[\mu_{34,L+1}\right]^{L+1}}{\left[\mu_{34,L}\right]^{L}}\widetilde{\lambda}_{34,L+1}-1}. \tag{45}$$

4.3.3 Simplifications

Interference-limited case: In an interference-limited environment, a simpler condition is obtained by omitting the "1"s corresponding to noise power in (43). Then, (43) reduces to

$$g_i < \left[\frac{\mu_{34,L+1}}{\mu_{34,L}}\right]^L \widetilde{\lambda}_{34,L+1}, \tag{46}$$

and (45) reduces to

$$R^n > \left[\frac{\mu_{34,L}}{\mu_{34,L+1}}\right]^L \left(\sqrt{M}+\sqrt{N}\right)^2 \frac{1}{\widetilde{\lambda}_{34,L+1}}. \tag{47}$$

Large transmit power: With large P_T, the power ratio approaches

$$\frac{\mu_{34,L}}{\mu_{34,L+1}} \rightarrow \frac{L+1}{L}, \tag{48}$$

which further simplifies the relation.

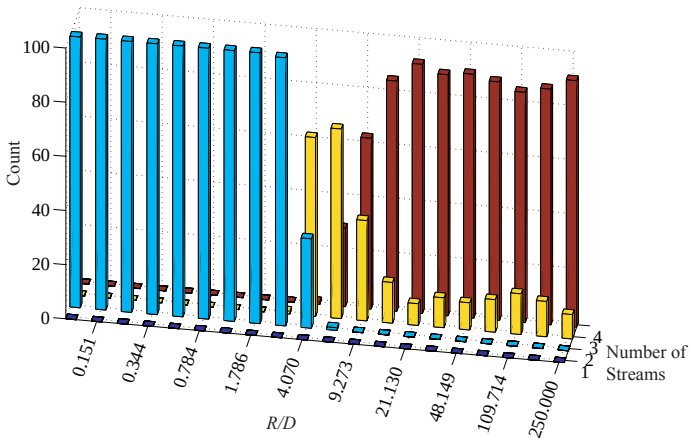

Figure 19: Histograms of number of streams used by one of the interfering CL-MIMO links with the distributed stream control algorithm for different R/D values.

4.3.4 Results

Figure 19 shows the histogram of the number of streams used when they are limited according to the criteria in (45). The total noise-normalized transmit power for each link is 20dB. With four antenna elements at each node, each link is assigned 2 streams initially. Each link checks to see if the condition in (45) is true to get one more stream.

Comparing Figures 19 and 16(a), we see that the stream control algorithm eliminates the use of excessive numbers of streams. The algorithm allows no additional stream for $R/D < 3$. The total number of streams never exceeds the globally optimum values shown in 16(b).

In the next chapter the throughput of interfering CL-MIMO links is analyzed. It is shown that the distributed stream control algorithm eliminates the throughput drop due to excessive streams.

We do not extend our analysis to large numbers of cochannel links in the neighborhood of a receiver, because that would correspond to a condition of receiver overload. We assume that the MAC would exert stream control so that the total number of strong streams is less than or equal to the number of antennas at each receiving node. In the discussion of the throughput improvement of multiple cochannel CL-MIMO

systems over time-division multiplexed and OL-MIMO systems in the next chapter we will also demonstrate the performance of the stream control algorithm with the three-link network of Figure 7. With more than two interfering links, the transmitters can practically apply the stream control algorithm on a link-by-link basis, or take into account only the closest link.

CHAPTER 5

THROUGHPUT IMPROVEMENT WITH INTERFERING MIMO LINKS

It is shown in [25,70] that with MEAs at both ends of a link, the bandwidth efficiency grows linearly with the number of antennas. This theory was validated by experimental demonstrations at Bell Labs, where bandwidth efficiencies of 30-40 bps/Hz were attained [31].

Traditionally if two wireless links would cause excessive interference on each other, they are assigned to different channels, e.g. they could be time-multiplexed. For instance, the IEEE 802.11 standard uses the CSMA/CA multiple access control (MAC) protocol. With this type of MAC, interference wouldn't be allowed. In the absence of interference and assuming the SNR is high and the fading correlation is low, the difference between OL and CL-MIMO capacities would be small. Therefore, all transmissions would use the OL-MIMO technique. Employing N antenna elements at each node would reduce the time required to transmit a packet of given size by a factor of N, thereby speeding up the whole system by N. This will be our baseline case and we refer to it as CSMA/CA(N).

However, the spatial filtering capabilities at both ends enable the MIMO links to operate co-channel with a higher network throughput than if they operated in a TDMA fashion. By network throughput we simply mean the sum of the Shannon capacities of links. The link adaptation and stream control algorithms introduced in the preceding two chapters make this improvement realizable.

Figure 20 illustrates the difference between the TDMA scheme and the non-TDMA

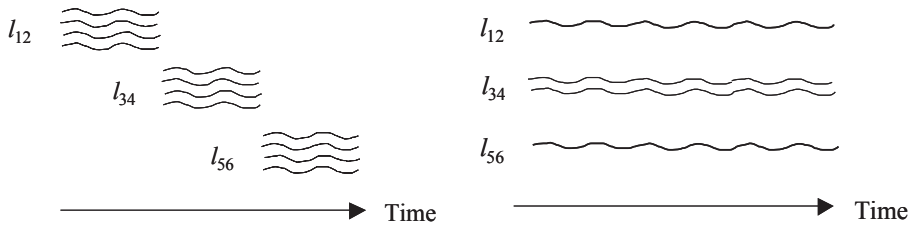

(a) MIMO-TDMA.

(b) MIMO with interference and stream control.

Figure 20: Illustration of TDMA operation and interfering MIMO links with stream control.

schemes with stream control for 3 links. Let the horizontal dimension be time. Each wavy line represents an independent data stream. In the TDMA scheme, each 4-element transmit array takes its turn to transmit four data streams. In either of the schemes with interfering OL- or CL-MIMO links, throughput is usually maximized if one transmit array is allowed two streams and the other two only have one stream each; this way, no 4-element receive array is illuminated by more than 4 streams.

Higher spectral efficiencies are possible with CL-MIMO than with OL-MIMO when there is interference. In this chapter we compare three MIMO schemes: OL-TDMA, OL with interference (OL-I) and CL-MIMO with interference (CL-I). "With interference" means that all three links are allowed to operate simultaneously. "TDMA" means the links operate in succession, and is intended to represent the CSMA/CA(N) protocol.

The percentage improvement over TDMA is calculated as

$$\frac{T - T_{TDMA}}{T_{TDMA}} \times 100\%,$$

where T is the average throughput with co-channel links, and T_{TDMA} is the average single-link capacity.

We will consider two approaches:

- With the fair-energy approach we constrain the total energy used by all schemes

to be equal. Notice that in Figure 20(a) each link uses its transmit power only during the allocated time portions. On the other hand, with OL-I and CL-I schemes, multiple links transmit continuously. For a fair comparison of the throughputs of different schemes, the transmit powers of the links in Figure 20(b) should be scaled by 1/3.[1]

- For the highest-throughput approach we assume that the links need the maximum throughput possible, regardless of the energy consumption. However, there are still constraints on the total transmit powers at each node. This case represents the improvements possible under heavy data traffic in a network.

5.1 Fair-Energy Approach

In this section we adjust the transmit powers of the links so that all schemes use equal energies.

5.1.1 Two-link Network

For the two-link network the noise-normalized transmit power is set to $P_T = 20$dB with the MIMO-TDMA scheme, and to $P_T{}' = P_T/2 = 17$dB for the schemes with interfering links. Each node has 4 antennas.

Figure 21 shows the average percent throughput improvement for several spatial multiplexing schemes relative to TDMA, based on a Monte Carlo simulation of 1000 channel trials. We first observe that OL-I yields lower throughput than OL-TDMA. The reason why OL simultaneous operation is worse than the TDMA case is similar to why V-BLAST is not as efficient as D-BLAST [14,31]. It is because different streams in OL-I originate from different transmitter arrays, therefore joint coding cannot be performed across all the antennas transmitting the streams.

[1]For maximum network throughput it might be necessary to allocate more power to l_{32}, however we treat each link equally in this analysis. The effect of different power allocation to the links was illustrated in Figure 12.

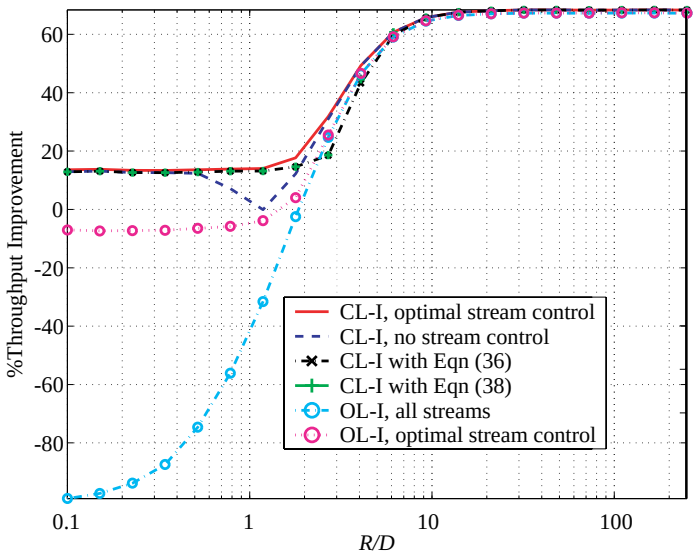

Figure 21: Throughput improvement analysis with the two-link network, fair-energy approach.

The CL-I is better than OL-I for $R/D < 2$ because the CL-I transmit array weight vectors are jointly adapted, not only to match their respective channels, but also to each other. In other words, each transmit array uses spatial filtering (beamforming) to avoid making interference on its unintended receiver while simultaneously providing transmit diversity to its intended receiver. We note that this advantage of jointly adapted CL-I over OL-I does not diminish with increasing SNR, in contrast to the MIMO-TDMA case.

The CSMA/CA protocol of 802.11 prohibits channel reuse if $R/D < 2$. Figure 21 shows that 15% to 25% improvement is achieved by the CL-I scheme relative to OL-TDMA for $R/D < 2$. The TDMA results apply to the CSMA/CA(N) protocol because CSMA/CA(N) would make one transmitter wait until another transmitter finishes, if they are close enough that their signals might interfere. It will be shown in the next section that we can get even better improvements if we are not concerned with the energy consumption, i.e. if we want to obtain the maximum possible network capacity.

The effect of receiver overload with the distributed adaptation methods without

stream control in the region $0.5 < R/D < 3$ is distinguished in the figure. As explained in the previous chapter, when $R \ll D$, the interference is strong enough that water-filling naturally blocks some of the channel modes. On the other hand, when $R \gg D$, all dimensions can be used despite the incoming interference. However, for $0.5 < R/D < 3$ there is a drop in the throughput because of the use of an excessive number of streams.

The throughputs with stream control according to (45) and (47) are close to that with optimal stream control in Figure 21.

5.1.2 Three-link Network

Next, we consider the three-link network of Figure 7(b), with $P_T = 20$dB for the MIMO-TDMA scheme, and $P_T{}' = P_T/3$ for the schemes with interfering links. Figure 22 shows the throughput improvements for the three-link network with four and three antenna elements at each node. For the case of four antennas at each node, one of the links is initially assigned two streams, and the other two are assigned one stream as illustrated in Figure 20(b). Each link can increase its number of streams if the distance to the closest interfered node satisfies the condition in (45) or (47). With three antennas at each node, each link initially is assigned one stream.

We observe that stream control is necessary for all values of $R/D < 3$, since at least one of the interfering transmitters is in the critical distance range. The stream control algorithm using either (45) or (47) gives nearly optimal performance. For small R/D, there is a small difference between the globally optimum stream control results and the results with the distributed stream control algorithm. This is because the initial choice of which link gets two streams is not optimal. Both of the plots in Figure 22 show that 20% to 50% improvement is achieved by the CL-I scheme relative to OL-TDMA for $R/D < 2$. Finally, the improvement of CL-I over OL-I with this network topology is 35% at high INR with four antennas, and 40% with

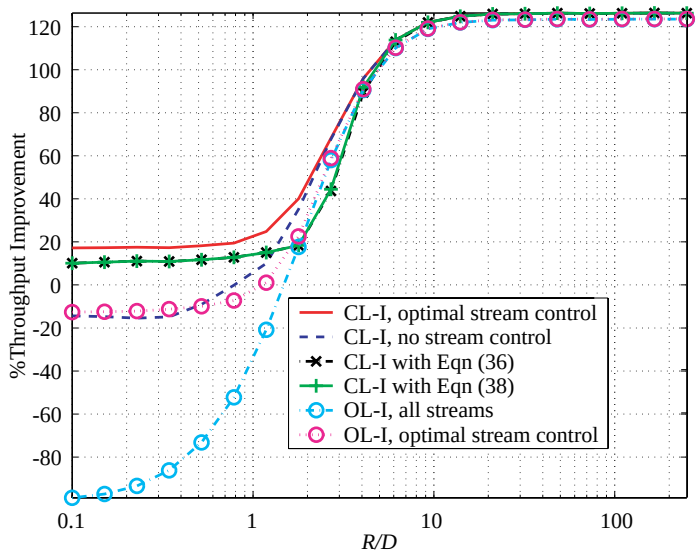

(a) 4 antennas.

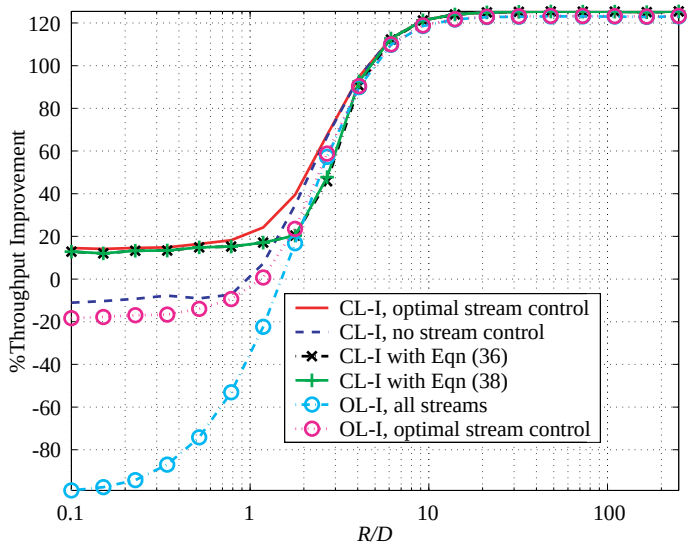

(b) 3 antennas.

Figure 22: Throughput improvement analysis with the three-link network, fair-energy approach.

three antennas.

5.2 Highest-Throughput Approach

In this section we assume each link uses its maximum transmit power. For all schemes the noise-normalized transmit power is set to $P_T = 20$dB.

5.2.1 Two-link Network

Figure 23 shows the throughput improvements with equal transmit powers. The improvements with this approach are higher than with the equal-energy approach because of the higher-energy advantage.

All schemes give similar results for low-power interference (large R/D). On the other hand, at high INR, or when R/D is small, CL-I gives over 20-22% improvement over OL-I with stream control. It is also shown that more than 30% improvement is achieved by the CL-I scheme relative to OL-TDMA for $R/D < 2$. Again, by limiting the number of streams according to the criteria in (45) and (47) the performances obtained are close to optimal, and the throughput drop due to excessive use of parallel streams in the range $0.5 < R/D < 3$ is eliminated.

5.2.2 Three-link Network

Figure 24 shows the throughput improvements for the three-link network with four and three antenna elements at each node, with equal transmit powers. The streams are initially assigned in the same way as explained in the previous section.

Both of the plots in Figure 24 show 40% to 70% improvement is achieved by the CL-I scheme relative to OL-TDMA for $R/D < 2$. The improvement of CL-I over OL-I is 25% at high INR with four antennas, and 30% with three antennas.

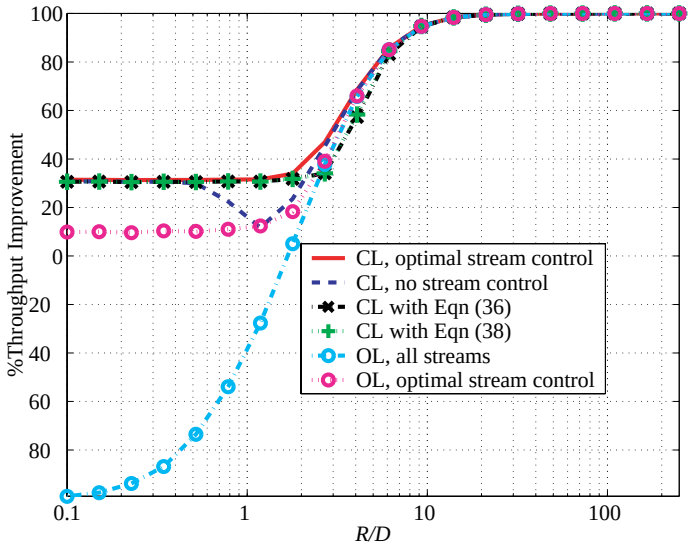

Figure 23: Throughput improvement analysis with the two-link network, highest-throughput approach.

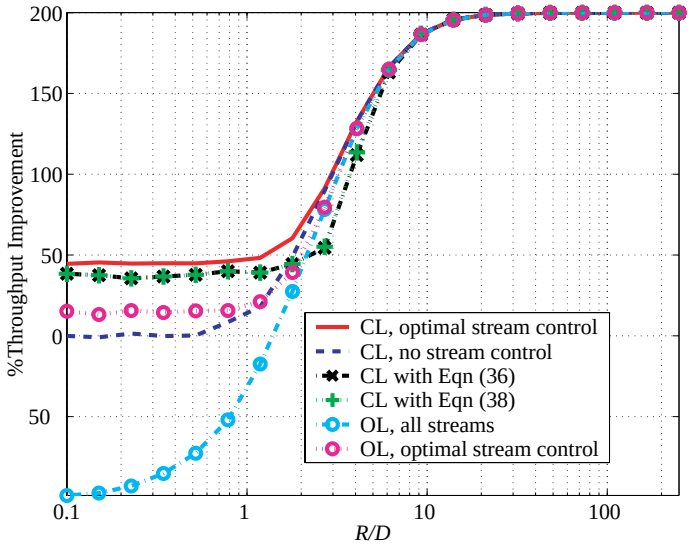

(a) 4 antennas.

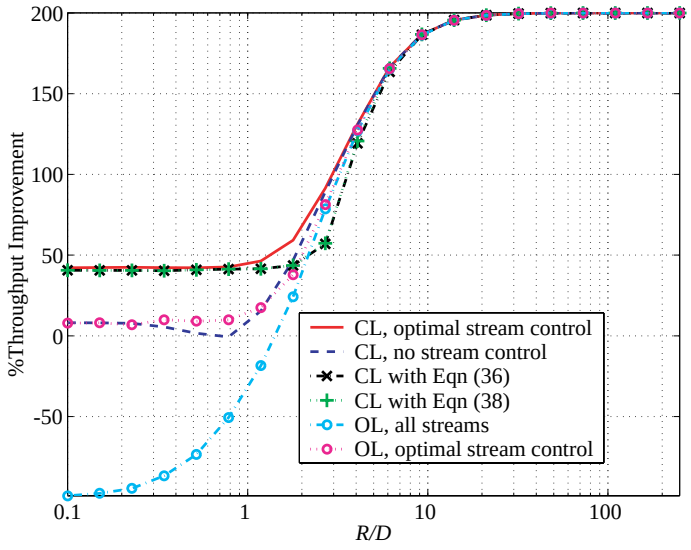

(b) 3 antennas.

Figure 24: Throughput improvement analysis with the three-link network, highest-throughput approach.

CHAPTER 6

RESULTS WITH CHANNEL MEASUREMENTS

So far we have considered simulated Rayleigh-fading channels. In this chapter, the performances of the MIMO links and the distributed link adaptation algorithms are demonstrated using measured data.

We consider several configurations corresponding to different channel and interference conditions. The configurations are selected to demonstrate the effects of the spatial correlation between data and interference streams, presence of line-of-sight (LOS), different path losses, and different scattering characteristics on the links' performance.

In the next section, we describe the measurement setup and the experiment. In Section 6.2 we discuss the effects of some environmental factors. In Section 6.3 we show the capacities with equal transmit powers for each link. In Section 6.4 we give some results assuming that the interfering links can adjust their transmit powers to achieve equal SNRs.

6.1 Measurement Setup and Experiment Description

We use channel measurements taken by virtual arrays, also known as synthetic arrays, at both ends of the link at the Residential Laboratory of Georgia Institute of Technology. The details of the measurement setup and the virtual array system can be found in [38]. We have extracted part of the data gathered for the experiments reported in [37].

Table 2: Four configurations considered to form networks of with two MIMO links with different channel and interference characteristics.

	Link 1	**Link 2**
Conf. I	T1-R1	T2-R2
Conf. II	T3-R1	T4-R2
Conf. III	T5-R1	T6-R2
Conf. IV	T5-R1	T7-R2

Virtual uniform linear arrays (ULA) with 4 elements are used at both the transmitter and the receiver. The antennas used at both sides of the links are omnidirectional, vertically polarized, wideband biconical antennas. The carrier frequency used is 5.8GHz, and the antenna spacing is half wavelength.

Each component of the channel matrix is in fact the wideband frequency response with bandwidth 500 MHz. The abundant frequency samples are utilized to increase the number of outcomes in the calculation of ergodic narrowband channel capacity. The number of frequency samples, 50, is chosen such that the separation between adjacent samples (10 MHz) is enough obtain independent channel realizations.

Figure 25 depicts the layout of the laboratory. As shown in the figure, there are two receive array locations and seven transmit array locations. We consider four configurations, each with two links, as summarized in Table 2. The node locations and network configurations demonstrate the effects of different environmental factors. We analyze these environmental factors in the next section.

We use two approaches to demonstrate both the performance of our CL-I scheme and the effect of the network topology. In the first approach, we keep the effects of the network topology and node distances. For each configuration, we scale the data channel for Link 1 so that each element of the channel matrix between T1 and R1 has unit variance. Then, we use the same scaling factor for the other data channel and the interference channels. Equivalently, we use the same transmit power for both

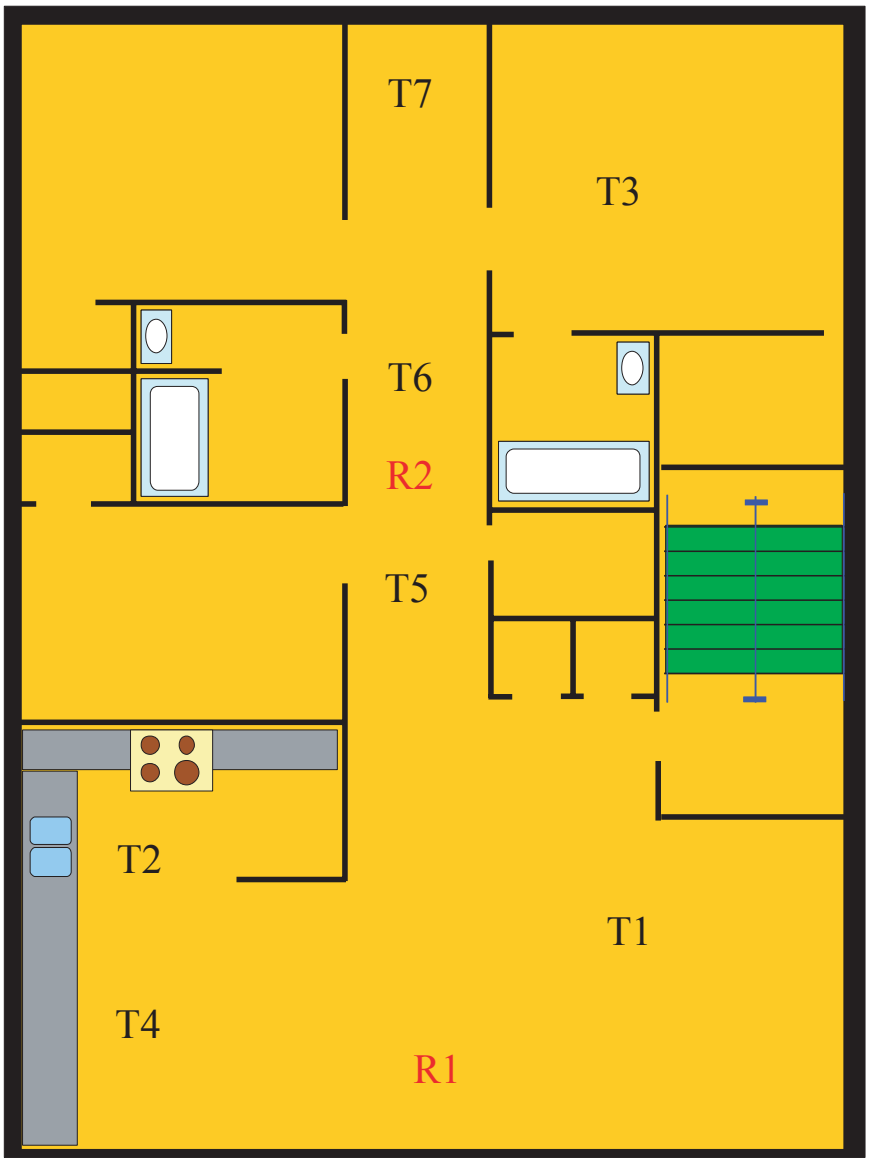

Figure 25: The layout of the Residential Laboratory.

links in each configuration. For instance, with Conf. I, the channel between T1-R1 has unit variance, and for Conf II, the channel between T3-R1 has unit variance.[1] With this approach, we can better observe the effects of LOS and node distances for a given configuration.

In the second approach, we normalize the data channel (i.e. the channel from the transmitter to the desired receiver) so that each coefficient of the channel matrix has unit variance, and use the same normalization factor to normalize the channel from the transmitter to the unintended receiver. With this approach, both links have the same transmit power, and the data channels have comparable gains in each configuration. However, we do not see some of the effects of the network topology.

6.2 Environmental Factors

Through different node locations and pairs of links, we analyze the effects of different environmental factors, such as the spatial correlation between data and interference streams, scattering characteristics and LOS, and different node distances.

The first two configurations correspond to less correlated interference conditions, because the directions of data and interference paths are angularly separated for both links. For the last two configurations the data and interference for both links are spatially more correlated. It will be shown in the next two sections that the throughput improvements of the CL-I scheme over TDMA for the configurations with spatially correlated interference is lower than the other configurations.

Tables 3 and 4 show the average channel mode gains of each link with no interference, according to the equal-transmit-power and equal-SNR approaches, respectively. The average is taken over 50 frequency samples. In Table 4, since the channel coefficients are normalized to have unit variance, the sum of the channel mode gains, or the

[1]Different configurations are still normalized separately. The results will not show the capacities of the links in one configuration relative to those in another.

Table 3: Channel mode gains of each link with no interference without normalization.

	T1-R1	**T2-R2**	**T3-R1**	**T4-R2**	**T5-R1**	**T6-R2**	**T7-R2**
λ_1	14.8074	0.0431	12.6046	43.2475	14.4319	32.2933	10.0765
λ_2	0.9936	0.0163	2.8207	14.0177	0.8170	11.5852	2.5693
λ_3	0.2071	0.0045	0.4879	4.0495	0.1609	3.7906	0.2850
λ_4	0.0094	0.0006	0.0369	0.5741	0.0121	0.1089	0.0184

Table 4: Channel mode gains of each link with no interference after each data channel is normalized separately.

	T1-R1	**T2-R2**	**T3-R1**	**T4-R2**	**T5-R1**	**T6-R2**	**T7-R2**
λ_1	14.8074	10.9011	12.6046	11.3523	14.4319	9.4976	12.3550
λ_2	0.9936	4.1259	2.8207	3.6796	0.8170	3.4073	3.1503
λ_3	0.2071	1.1325	0.4879	1.0630	0.1609	1.1148	0.3495
λ_4	0.0094	0.1479	0.0369	0.1507	0.0121	0.0320	0.0225

expected value of the trace of the channel gain matrix $\mathbf{HH}'$ would be 16. However, since only 50 samples are used and the normalization is done over each element of the channel gain matrix, the sum of each column in the table is not exactly 16.

To illustrate the difference of the two approaches and to better understand the advantage of LOS, consider Conf. I. The channel of Link 1 (T1-R1) has a LOS, and the transmitter-receiver distance is short, while the channel gain for Link 2 (T2-R2) is lower because it is longer and goes through a wall. The trace of the channel gain matrix $\mathbf{HH}'$ for Link 2 is lower than Link 1 by a factor of 24dB. However, with the equal-SNR approach, we assume Link 2 can use more power to achieve the desired SNR.

Looking at Table 4, we see that the links with LOS, such as T1-R1 and T5-R1, have one strong mode and three weak modes, whereas the non-LOS (NLOS) links, T2-R2 and T4-R2, each have three modes that have gains greater than one. This does

not mean links T2-R2 and T4-R2 have higher capacities than T1-R1 and T5-R1; LOS is a favorable condition. However, the improvement that can be obtained with MIMO operation in rich-scattering environments is higher.

On the other hand, link T6-R2 also has multiple strong channel modes, although it is a LOS channel. This is because the distance between the nodes is small and it is in a hallway, thus, the fading coefficients between different transmit and receive antenna pairs are fairly uncorrelated.

Finally, we note that with highly dissimilar channel gains, a globally optimum stream control would completely shut off the weaker link. However, we give two streams to each link. Then using the stream control algorithm given in Chapter 4, we allow additional streams to maximize the network throughput. Power control among the links would also help the links to have fair utilization of the wireless channel.

6.3 Results with Equal Transmit Powers

Table 5 shows the capacities of the links for several schemes developed in this dissertation and for each network configuration. We assume the two links use equal transmit powers in each configuration. We also assume that the schemes with interfering links have half the transmit power (17dB) of the TDMA schemes (20dB) so that all schemes use the same energy. Note that with the TDMA schemes, the links transmit half of the time (assuming equal priorities), so the values shown in the table for OL- and CL-TDMA are half of the link capacities computed based on the peak total power per link.

Even though the channels of Link 1 in all configurations are normalized to have the same total gain, the capacities of these links are not the same. Link 1 of Conf. II (T3-R1) has the highest capacity. Link 1 of Conf. I, III, and IV have a LOS, whereas the Link 1 of Conf. II does not. Normally, the LOS links would have a higher capacities because they have higher SNR. However, after normalization, the capacity of the

Table 5: Capacities in bps/Hz of different MIMO schemes and network configurations assuming equal transmit powers.

		OL-TDMA	CL-TDMA	OL-I with Stream Control	CL-I with no Stream Control	CL-I with Stream Control
Conf. I	**T1-R1**	7.9141	8.3620	11.9757	12.9414	13.1456
	T2-R2	0.8450	1.2763	0.5741	1.3071	1.2986
Conf. II	**T3-R1**	9.2249	9.4853	7.3796	11.5840	10.6092
	T4-R2	14.0573	14.0947	18.3677	16.7216	19.3601
Conf. III	**T5-R1**	7.5675	7.9779	3.8580	6.7857	5.3343
	T6-R2	12.8981	13.0340	16.0863	12.1803	16.7479
Conf. IV	**T5-R1**	7.5675	7.9779	6.4470	8.4682	8.4447
	T7-R2	8.5250	8.8912	9.8485	8.4372	10.2116

NLOS link is higher because the channel gain is not concentrated in just one mode. The capacities of the LOS links with normalized path loss gains (Link 1 in Conf. I, III, and IV) are close to each other.

For each configuration, one link has more path loss than the other, resulting in lower capacity for the link with more loss. When there is interference, that is, when both links operate simultaneously, we observe that the switch from OL to CL gives the weaker link a much larger percentage increase in capacity than it gives the stronger link. For example, in the Conf. III "with stream control" cases, the improvement that CL-I gives over OL-I is 53% for the weaker link (Link 1, T5-R1), but only 4.1% for the stronger link (Link 2, T6-R2).

Some insights can be gained by looking also at the TDMA or no-interference cases. In those cases, the change from OL to CL usually does not make a big improvement for the weaker link. The exception is Conf. I, Link 2 (T2-R2). We expect a big difference between OL-TDMA and CL-TDMA only when the SNR is low, which must be the case for Conf. I, Link 2 (T2-R2). Therefore, in this particular case the difference

between OL-I and CL-I is attributable mostly to low SNR, and not so much to better control of the interference.

On the other hand, in the weaker links where OL-TDMA and CL-TDMA give about the same performance, we can conclude that their SNRs must be high, and the other link in each configuration has an even higher SNR. However, because there is a big difference between OL-I and CL-I, we may conclude that under OL-I, the weaker link has a low signal-to-interference ratio (SIR), and the improvement from CL-I is attributable to the spatial filtering doing a good job of interference management.

It is also interesting to compare CL-TDMA and CL-I with stream control. In the first two configurations, the strong link gets a large improvement and the weak link gets a small improvement. These configurations have interference that is not highly spatially correlated with the desired signal, so jointly optimized spatial filtering is effective at managing the interference. The latter two configurations have spatially correlated interference. This leads to minimal improvements in throughputs. In Conf. III, the interference seen by the weak link (T5-R1) is so correlated and strong that the capacity of the link actually degrades in CL-I. We conclude that when the interference is spatially correlated with the desired signal, spatial filtering does not provide good interference management.

6.4 Results with Equal SNRs

Assuming that the two links have equal SNRs in each configuration, we compare the throughputs of the schemes considered in the previous section.

Normalizing each transmitter's total power to obtain equal SNRs may not be practical in all configurations. For instance, in Conf. I, Link 2's transmit power has to be 24dB higher than Link 1. However, we follow this approach to give the links comparable capacities in our throughput comparisons.

Again, we constrain the total transmit energies to be equal for TDMA and spatial

Table 6: Whitened channel mode gains when both links transmit with 17dB noise-normalized power.

	Conf. I		**Conf. II**		**Conf. III**		**Conf. IV**	
	T1-R1	**T2-R2**	**T3-R1**	**T4-R2**	**T5-R1**	**T6-R2**	**T5-R1**	**T7-R2**
$\widetilde{\lambda}_1$	2.6878	2.7880	3.1404	2.6348	1.1705	2.1791	1.6738	2.5194
$\widetilde{\lambda}_2$	0.6391	1.5675	1.1771	1.2395	0.5508	1.0358	0.5301	0.8345
$\widetilde{\lambda}_3$	0.0318	0.7204	0.0653	0.1911	0.2692	0.2252	0.2208	0.1954
$\widetilde{\lambda}_4$	0.0011	0.1950	0.0024	0.0108	0.0781	0.0200	0.0536	0.0095

Table 7: Whitened channel mode gains when both links transmit with 7dB noise-normalized power.

	Conf. I		**Conf. II**		**Conf. III**		**Conf. IV**	
	T1-R1	**T2-R2**	**T3-R1**	**T4-R2**	**T5-R1**	**T6-R2**	**T5-R1**	**T7-R2**
$\widetilde{\lambda}_1$	2.9243	3.0776	3.2042	2.7800	1.8486	2.3306	2.2909	2.7235
$\widetilde{\lambda}_2$	0.7222	1.8560	1.2836	1.3760	0.7729	1.1144	0.6821	0.9401
$\widetilde{\lambda}_3$	0.1006	0.9469	0.1749	0.3904	0.3636	0.2904	0.3188	0.2808
$\widetilde{\lambda}_4$	0.0035	0.3078	0.0079	0.0354	0.0945	0.0530	0.0852	0.0263

multiplexing with interfering links. The results are shown for two power settings: high-SNR, and low-SNR. With the high-SNR setting, the noise-normalized transmit power for TDMA links is 20dB, while for the schemes with interfering links, it is 17dB because of the equal-energy argument. With the low-SNR setting, the noise-normalized transmit power for TDMA links is 10dB, and for the schemes with interfering links, it is 7dB.

Tables 6 and 7 show the whitened channel mode gains when both links transmit simultaneously with 17dB and 7dB noise-normalized power, respectively. The gains are obtained after the power-controlled link adaptation method with the distributed stream control algorithm. Each link is initially assigned two streams.

Table 8: Throughputs in bps/Hz of different MIMO schemes with high SNR (20dB for TDMA schemes, and 17dB for schemes with interference).

	OL-TDMA	**CL-TDMA**	**OL-I with Stream Control**	**CL-I with no Stream Control**	**CL-I with Stream Control**
Conf. I	18.4721	19.0306	20.9420	22.6106	24.6570
Conf. II	19.7030	20.0722	21.1701	25.1391	25.5378
Conf. III	17.4234	18.1287	16.2264	16.2889	18.5827
Conf. IV	16.5504	17.2994	16.7787	17.2787	19.1082

Comparing the isolated channel mode gains in Table 4 with the whitened mode gains in the high-SNR setting in Table 6, a significant drop is seen because of the interference. The interference considerably degrades the channels. However, since the dependence of the capacity on the channel gain is logarithmic, we still see some throughput improvement with interfering MIMO links.

When the transmit power is reduced from 17dB to 7dB, the whitened channel mode gains increase, since the interference power seen by each link is reduced. However, the difference of the values shown in Tables 6 and 7 is very small, compared to the difference of these values with the isolated channel mode gains. With spatial filtering at both the transmitter and the receiver, and stream control, the desired streams of a link are not drastically effected by the power of the interference. This result shows that stream control is a key factor for the performance of interfering MIMO links.

Tables 8 and 9 show the network throughputs for each configuration obtained by several schemes. Since the links have comparable gains with the equal-SNR approach, the network throughputs are shown for each configuration, rather than individual link capacities. Table 8 shows the high-SNR results, and Table 9 shows low-SNR results.

The improvement of closed-loop operation over open-loop is not very large for

Table 9: Throughputs in bps/Hz of different MIMO schemes with low SNR (10dB for TDMA schemes, and 7dB for schemes with interference).

	OL-TDMA	**CL-TDMA**	**OL-I with Stream Control**	**CL-I with no Stream Control**	**CL-I with Stream Control**
Conf. I	8.9672	9.9283	10.5507	12.8231	13.5425
Conf. II	9.6016	10.4802	10.2771	13.1696	13.4744
Conf. III	8.4184	9.5296	7.9352	9.4560	10.1111
Conf. IV	7.9556	9.1317	8.4899	9.9173	10.5278

isolated links. Going from OL- to CL-TDMA gives only 1.8–4.5% improvement at 20dB SNR. At 10dB, the improvement ranges from 7% to 14.7%. However, with interference, the difference is more significant. With stream control, CL-I is 13.9% to 20.6% better than OL-I at high SNR, and 24% to 28.6% at low SNR. Therefore, closed-loop operation becomes rewarding with low SNR or interference.

The high SNR throughputs in this section can be compared with the throughputs calculated from Table 5, for the topology-preserving normalization. From Table 5, the throughput improvements for OL- to CL-TDMA are 10.04%, 1.28%, 2.67%, and 4.83%, by order of configuration. The only noteworthy difference between these values and the improvements of Table 8 is for Conf. I, which has a LOS link (T1-R1), and a low-SNR link (T2-R2) with the topology-preserving normalization. Thus, both links benefit from closed-loop operation in this configuration.[2] In Table 8, the SNR of T2-R2 is more (by 24dB), and since the channel of this link does not have a LOS, the open- and closed-loop capacities are closer to each other.

In Table 5, the improvements for OL-I to CL-I with stream control are 15.10%, 16.40%, 10.72%, 14.49%, in order of configuration. These numbers are lower than the

[2]The LOS link improves with CL becauseof the disparity in the mode gains.

improvements for Table 8, for equal SNR. This is because in the topology-preserving case, the biggest percentage capacity improvements occur for the weaker link. When the capacity improvements of the weak and strong links are added to get the improvement, the percentages are not as high as in the equal-SNR case.

We recall from the simulated results of Figures 21 and 22, that OL-I with stream control yields lower throughputs than OL-TDMA for strongly interfering links. In all three cases, that is, in Tables 5, 8, and 9, Conf. III is the only one that falls into this category of "strongly interfering links." In Conf. IV, the other correlated interference configuration, OL-TDMA and OL-I throughputs are nearly equal. In Conf. I and II, OL-I throughputs are higher by 7% to 43% than OL-TDMA. This suggests that the "strongly interfering" scenario may be unlikely in indoor environments.

Of course, the most dramatic differences in throughput are between CL-I with stream control and OL-TDMA. Of these, the low-SNR cases in Table 9 yield the highest improvements as a group: 51.02%, 40.33%, 20.11%, and 32.33%, in order of configuration. However, the single highest improvement in throughput is for Conf. I with the topology-preserving normalization: 64.90%.

In summary, if the desired and interfering transmitters are resolvable by the receivers, spatial multiplexing of interfering MIMO links, in combination with stream control and transmit prefiltering, gives significant improvement over time-division-multiplexing.

CHAPTER 7

PRACTICAL CONSIDERATIONS

The performance and throughput improvement results presented in the earlier chapters neglect some of the practical issues such as CSI aging, and the overhead of iterative joint link adaptation. In this chapter we analyze these effects, particularly for the IEEE 802.11b standard, and consider noniterative suboptimal solutions to the joint link adaptation problem.

7.1 Nonstatic Channel

So far we have assumed that both the transmitter and the receiver nodes of a MIMO link have perfect CSI. This is only possible if the channel is static for the burst duration. The transmitter can obtain CSI only at certain time intervals, through feedback, or, in TDD systems with no interference, through reception of signals in the reverse channel. Therefore, for closed-loop operation the block-fading assumption must be valid for substantial amounts of time.

If CSI ages rapidly, the transformation used at the transmitter to uncouple the parallel streams and the optimum power allocation will not match the channel realization at a later time instant. Channel mismatch can cause the transmit power to be concentrated in undesired directions, and allocated to the weaker modes, thereby, causing the performance to drop even below that of an OL-MIMO link.

Hence, CSI aging effects the performance of the links and determines if the closed-loop operation is feasible. In this section we analyze the effect of CSI aging for MIMO links.

7.1.1 Simulation Model

To analyze the effect of CSI aging, we use the fading channel simulator introduced in Section 2.5.2. We assume that the channel is estimated at the receiver at time $t = 0$, CSI-feedback is sent instantaneously to the transmitter, and the transmitter weights are frozen.

We assume that the receiver can track the channel at all times.[1] This can be done via transmission of pilot symbols or with adaptive equalization techniques. The problem of MIMO channel tracking at the receiver with training signals was studied in [32, 48, 64, 65], and reviewed in Section 2.7. It was illustrated in [65] that with the minimum required training length (with number of symbols equal to the size of transmit array) and simple time-interpolation of the channel coefficients the channel can be estimated fairly well despite large processing delays.

The channel varies according to (15). The channel $\mathbf{H}_p$ at time $p\tau$ has a component known by the transmitter, given by $\zeta^p \mathbf{H}_0$, and with correlation decaying as ζ^p, and an unknown component, growing in time as $1 - \zeta^p$. For $p \to \infty$ the channel becomes totally random to the transmitter.

Note that this model does not account for abrupt changes in the channel gains because of different shadowing characteristics.

7.1.2 Feasibility of Closed-Loop Operation

7.1.2.1 Isolated MIMO Link

For an isolated link, the difference between closed-loop and open-loop capacities is small, especially at high SNR and in a rich scattering environment. Moreover, the autocorrelation of the optimum transmit weight vectors (the columns of $\mathbf{V}$) drops sooner than the autocorrelation of channel matrix coefficients [43]. Therefore, the

[1] A MIMO link is considered for low-mobility systems, where at least the receiver can reliably track the changes in the channel statistics.

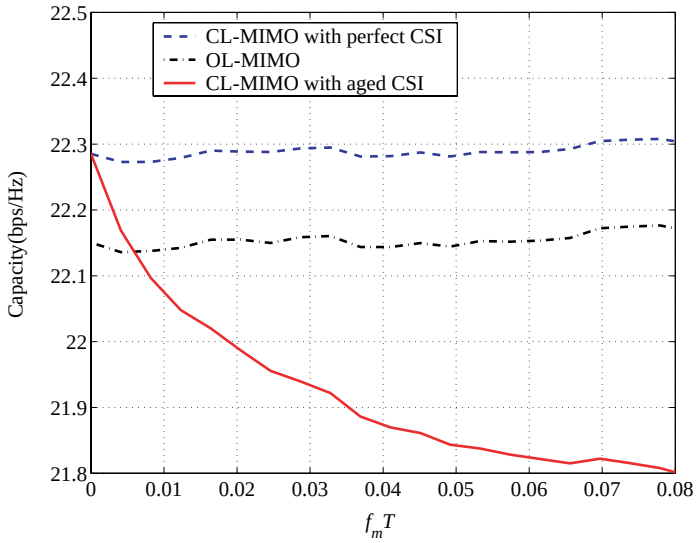

Figure 26: The effect of mobility on the performance of an isolated CL-MIMO link.

performance with aged CSI at the transmitter falls below that of OL-MIMO quickly.

Consequently, the closed-loop operation of an isolated link is feasible only for channels with very low Doppler frequency, or short frame length. According to [43], at a Doppler frequency of 40Hz, the required channel update rate is 0.18ms.

Figure 26 shows the average capacity of an isolated MIMO link as a function of $f_m T$ for three cases: CL-MIMO with perfect CSI at the transmitter at all times, OL-MIMO, and CL-MIMO with aged CSI at the transmitter. We observe that the curves are very close to each other. This is just an example of how CL and OL yield similar results without interference at high SNR. The capacity of CL-MIMO with aged CSI drops under the OL capacity at $f_m T = 0.006$, or in 0.15ms at 40Hz Doppler frequency, which supports the result of [43].

7.1.2.2 Interfering Links

With a set of cochannel MIMO links, the difference between closed-loop and open-loop capacities is larger than with isolated MIMO links. In addition, even partial knowledge of the CSI at the transmitter helps to null interference, as well as to decouple the streams. Therefore, the performance with aged CSI at the transmitter

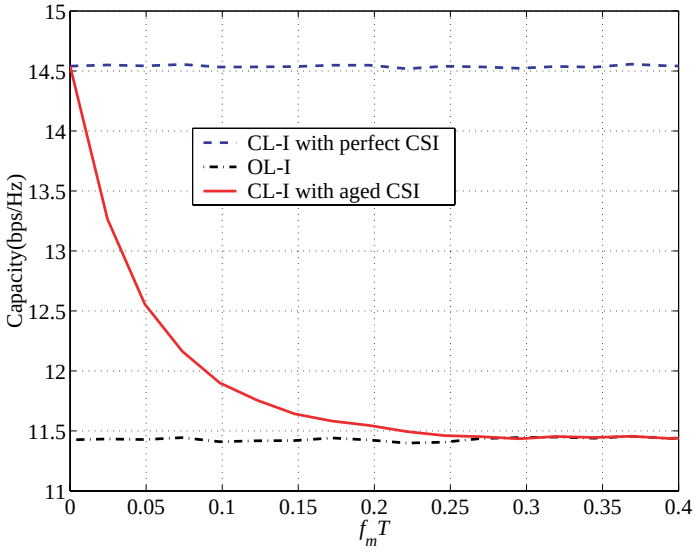

Figure 27: The effect of mobility on the performance of two CL-I links when each of the links of Figure 7(a) gets two streams, and the noise-normalized transmit power is 20dB.

does not fall below OL-MIMO capacity as quickly as in the case of isolated links.

To illustrate this, we consider the two-link network of Figure 7(a) with equal node distances ($R = D$), 4 antennas at each node, 2 streams per link, and 20dB noise-normalized transmit power at each node. Figure 27 compares one link's capacity for the following three scenarios: CL-I assuming perfect CSI at the transmitter at all times, OL-I, and CL-I with frozen weights. We observe that the closed-loop performance is better than open-loop for $f_mT < 0.3$.

For this experiment, the throughput with frozen weights degrades down to the OL-I throughput. However, this is not always the case. Figure 28 shows the same throughput comparison for both links when link l_{12} transmits through one stream, and l_{34} gets three. The transmit power is reduced to 10dB to better visualize the difference of the performance of CL-MIMO from OL-MIMO because of nonuniform power allocation to the channel modes. In this case the throughput with frozen weights degrades below OL-I throughput for l_{34} as the transmitter's CSI ages. This configuration also shows that the performance of the CL-I scheme with aged CSI at

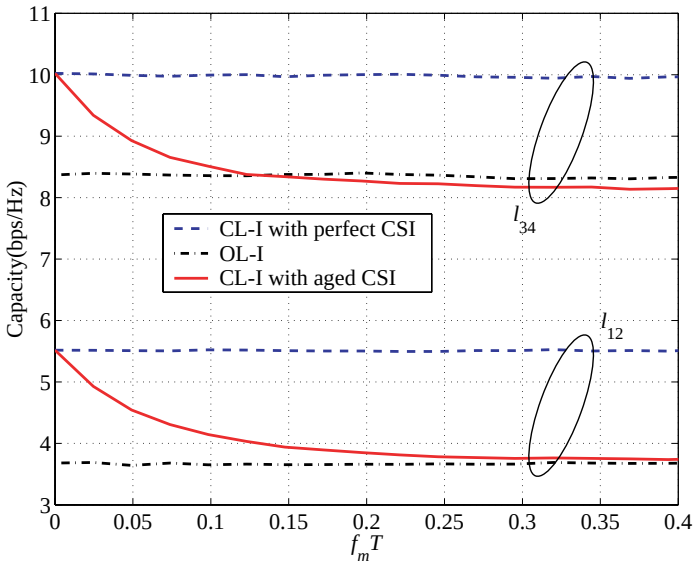

Figure 28: The effect of mobility on the performance of two CL-I links when one of the links of Figure 7(a) gets one stream, and the other gets three streams. The noise-normalized transmit power is set to 10dB.

the transmitter does not fall below OL-I capacity as quickly as in the case of isolated links.

7.1.3 Performance Comparison of OL-I and CL-I with Aged CSI

In this subsection we explain why the performances of CL-I with aged CSI at the transmitter and OL-I are sometimes nearly equal and sometimes different.

In a CL-MIMO link with aged CSI, the transmitter will use the SVD of the available channel, $\mathbf{H}_0$. The unitary transformation applied to the signals on the transmitter side is the matrix with the right singular vectors, $\mathbf{V}_0$. Thus, the received signal at time pT before any receiver processing is

$$\mathbf{y} = \mathbf{H}_p \mathbf{V}_0 \mathbf{\Sigma}_0^{1/2} \mathbf{x} + \mathbf{n}, \tag{49}$$

where Σ_0 is the diagonal matrix of power coefficients for each stream of the link, calculated according to $\mathbf{H}_0$.

It is shown in [49, 70] that if $\mathbf{H}$ is an $M \times N$ complex Gaussian matrix with

independent identically distributed entries, and each entry has independent real and imaginary parts with zero mean and equal variance, then for any unitary $M \times M$ matrix $\mathbf{U}$ and unitary $N \times N$ matrix $\mathbf{V}$ the distribution of $\mathbf{UHV}'$ and $\mathbf{H}$ are the same.

Therefore, with our statistical channel simulation model, $\widehat{\mathbf{H}}_p = \mathbf{H}_p\mathbf{V}_0$ has the same distribution as $\mathbf{H}_p$. As $p \to \infty$ and the channel becomes totally random to the transmitter, the difference in the average capacities of CL- and OL-MIMO links is only because $\mathbf{\Sigma}_0$ is not a scaled identity matrix, that is, $\mathbf{\Sigma}_0$ is not optimal for OL-MIMO. For the configuration of Figure 27 the SNR is high, and each link uses a only 2 streams (with large gains that are close to each other). Thus, the throughput with frozen weights does not fall noticeably below the OL-I throughput.

With the low-SNR configuration considered in Figure 28, the throughput of link l_{12} does not fall below OL-I throughput as well, since the link uses only one stream. However, for l_{34} the power levels of the 3 streams with disparate gains deviate more from uniform, and the average capacity falls below that of OL-I.

In the case of an isolated MIMO link, the performance difference is more noticeable. In this case, all four streams are utilized, and they have more disparate gains.

7.1.4 Analysis of Time Overhead and Mobility Based on the 802.11b Standard

At the 11-Mbit/second rate for 802.11b, a packet takes about 1 millisecond of air time [10]. It can be seen from Figure 27 that after 1ms at 40Hz Doppler frequency ($f_m T = 0.04$), the CL performance is still 12% better than the OL performance. With a carrier frequency of 2.4GHz used by 802.11b, this would correspond to a mobile speed of 20km/h. At pedestrian speed (up to 10km/h) it takes 2ms until the improvement drops to 12%. However, this neglects the overhead of the time spent for iterative link adaptation.

According to the 802.11b standard, typical RTS and CTS and data packet sizes, in order, are 44, 38, and 512 bytes. Using small packets is preferable because of the high BER of a radio link, and the retransmit overhead in case of packet corruption. Assuming a data packet size of 512B, the transmission time of a packet is 0.36ms at the 11Mb/s mode, and 0.72ms at the 5.5Mb/s mode.

We assume that the CSI is piggy-backed in the CTS packet. Assuming a nondispersive 4×4 channel, the complex Hermitian matrix $\mathbf{H}'\mathbf{H}$ can be represented by 16 real numbers.[2] With "single" precision[3] an additional 64B is sufficient for CSI feedback.

It was shown in Section 3.3 that the median of the number of iterations required for the power-controlled joint link adaptation method to converge is 6 with two links, and 9 with three links. Although the most improvement takes place in the first two-three iterations, the improvement of CL-I is inadequate to offset the overhead of the iterative joint link adaptation process unless the channel is static and multiple packets are to be transmitted with the same configuration. Therefore, closed-loop operation of MIMO links is feasible only for fairly static channels.

We observed in Chapter 3 that the most improvement in throughput takes place in the first iteration or the first two iterations. In a static environment, the data packets can be transmitted suboptimally until convergence. Assuming all the links keep exchanging packets, then further improvement may be reached with more iterations. This kind of operation could eliminate exchange of extra control messages.

For an isolated link, the performances with open- and closed-loop operation are very close at high SNR, and CSI aging brings the CL-MIMO throughput below OL-MIMO quickly even at low Doppler frequencies. For CL-I links, the iterative link

[2]The eigenvalue decomposition of $\mathbf{H}'\mathbf{H}$ gives the channel mode gains, as well as the transmit weight vectors.

[3]The data type of IEEE Single is represented by 32 bits, 8 of which are exponent bits.

optimization creates an overhead. In the next section, we consider noniterative suboptimal solutions.

7.2 Noniterative Suboptimal Solutions

As shown in the previous section, CL-I operation is feasible only for static channels, due to the overhead of the iterative link adaptation process.

One way to eliminate the need for iteration is to assume that the interference is white; this was the assumption in [23]. With this assumption, the links would use the power coefficients and transmit weight vectors calculated for the nonwhitened channel. This assumption would be valid for large numbers of interferers. However, we do not allow receiver overload in our model, and the interfering streams are limited by the DOFs at the receiver nodes. In this case, the interference is actually nonwhite [44, 62]. In addition, it was shown in Chapter 4 that stream control is the key to the performance of the interfering MIMO links.

In this section, we consider three noniterative solutions for the closed-loop operation of cochannel links. The first one, given in [23], assumes that the interference is white. We develop another solution based on the idea of [23], but also include stream control. For the third solution, each transmitter determines its parameters assuming that the interfering links are open-loop. To illustrate, let's consider the two-link network of Figure 7(a). Assuming that each node uses two streams, and that node 1 knows $\mathbf{H}_{32}$ as well as $\mathbf{H}_{12}$, it estimates the interference correlation matrix seen at node 2 as

$$\widehat{\mathbf{R}}_{32} = \mathbf{H}_{32}\widehat{\mathbf{P}}_{12}\mathbf{H}'_{32} \tag{50}$$

where the first two diagonal elements of $\widehat{\mathbf{P}}_{12}$ are $P_T/2$, and the other elements are zero.

Figure 29 shows the CDFs of the throughputs obtained with these noniterative

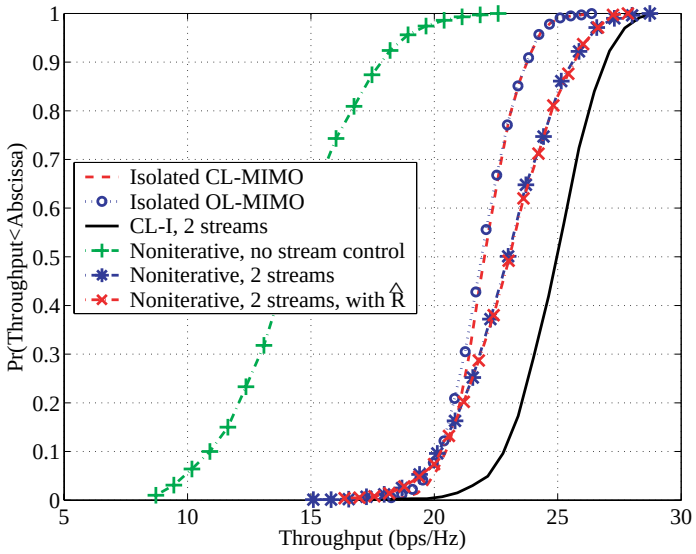

Figure 29: Performance with the noniterative suboptimal solutions.

solutions for the two-link network, with 4 antennas at each node, and equal node distances ($R = D$). Isolated OL-MIMO and CL-MIMO capacities, and the throughput of CL-I (with two streams at each link) are also shown for comparison. For the isolated link capacities, the noise-normalized transmit power is 20dB, and for the throughput calculations with interfering links, it is 17dB. The performance with the first noniterative solution (without stream control) is worse than the TDMA throughput given by the isolated link capacities. The second noniterative solution (with stream control) can be worse than TDMA in some cases, but the throughput with this approach gives 4.63% average improvement over CL-TDMA. Finally, estimating the interference as illustrated in (50) does not improve the performance.

CHAPTER 8

SUMMARY AND FUTURE WORK

In this chapter, we summarize the research results and contributions, and suggest directions for the future work.

8.1 Research Summary

The research reported in this dissertation has given us an in-depth understanding of the flexibility and performance enhancement that MIMO links can provide, and the challenges they bring for an effective utilization of the resources in a network.

We have developed methods of joint adaptation of link parameters for a set of flat-fading cochannel CL-MIMO links. Using transmit power, desired capacities, or the number of parallel streams for each link as control parameters, these algorithms enable the MIMO links to operate co-channel with a higher network throughput than if they operated in a TDMA fashion. Moreover, the control parameters used by the algorithms provide allow us to control the capacity of each link according to different data rate or QoS requirements.

The algorithms are distributed, and can be used in ad hoc networks. The simplicity and the fast convergence of these algorithms make them attractive even for centrally controlled networks.

This research has demonstrated the potential throughput improvements of simultaneous operation of cochannel CL-MIMO links. The analysis made with sample two- and three-link networks and simulated channels suggests that the closed-loop operation schemes may be desirable in applications with slowly varying CSI.

The performance of the new algorithms was also demonstrated by measured channels. Several network configurations with different channel and interference conditions and various power settings showed that power and stream control both play key roles in the fair utilization of the wireless resources. The power control is essential both among the links and the streams of each link. Although all measurements were taken in the same building, different LOS and path loss characteristics of the links produced disparities as high as 24dB in the channel gains.

The CL-I scheme with stream control gave improvements over TDMA even when the interfering links were spatially nonseparable by directional arrays.

Although with the simulated Rayleigh fading channel model spatial multiplexing with OL-MIMO links did not appear to be a favorable scheme, with the measured channels the performance of OL-I with stream control was better than OL-MIMO in three out of four configurations.

The effect of CSI aging at the transmitter and the overhead of the iterative joint link adaptation were analyzed. The gain of closed-loop operation for an isolated MIMO link drops quickly with CSI aging. However, the links with interference have higher difference between their OL and CL capacities, which gives more room for CSI aging. This makes the CL-I operation feasible for static and low-mobility networks.

To remove the overhead of the iterations with the distributed link adaptation algorithms, a noniterative solution was given that uses stream control and assumes white interference. Although the performance with this solution can be worse than TDMA in some cases, on average, the CL-I operation gives an improvement (4.63% for the two-link network with equal node distances) over CL-TDMA.

The appropriate MAC layer that would exploit the throughput improvement with interfering MIMO links is different from the current standards, such as 802.11, which enforces time sharing among links that would interfere. The research results and the resource allocation methods build a baseline for future multiple-access control (MAC)

layer designs.

8.2 Suggestions for Future Work

The goal of the reported research is to to develop a reliable joint link optimization algorithm which incorporates closed-loop MIMO with interference. Some directions for research to follow our joint link optimization algorithms are:

- **Dynamics of the adaptive process:** Convergence properties of the iterative algorithms were analyzed for initialization of the link weights. Another important issue is the change in the capacities after abrupt perturbations, such as changes in the number or locations of the interference streams, or changes in the channel because of mobility.

  Modelling the adaptation process in more detail to capture the receiver signal processing, the asynchrony of the packet transmissions, the time-varying flat-fading channels for all links, and the signaling of CSI may yield ways to speed up the convergence.

- **CSI feedback signalling:** The CSI feedback creates a major overhead for our physical layer algorithms. In the presence of interference, alternative ways such as learning the channel from the previous reverse-link transmission in TDD are not optimal. One node cannot know the interference sensed at another node without some signaling of that information. Strategies to minimize the feedback signaling overhead are needed.

- **Nonlinear receiver processor algorithms:** The whitening operation in (12) assumes linear processing to suppress interference, and that the interfering signals are unknown to the receiver. However, MUD techniques that detect the interfering streams may allow more cochannel streams and yield better throughputs.

- **Designs of MAC protocols:** The algorithms introduced in this dissertation allow multiple cochannel MIMO links to operate simultaneously with higher throughput than with time-multiplexing schemes. New MAC protocols are needed to facilitate this kind of operation and support the necessary control information exchange.

- **Frequency selective channels:** This thesis addressed only the flat-fading channel, however, many existing standards are for frequency selective channels. For instance, in an 802.11b receiver, the spreading code enables significant interference suppression. The algorithms in this thesis can be extended to two dimensions, space and time or space and frequency.

REFERENCES

[1] Al-Dhahir, N. and Diggavi, S. N., "Maximum throughput loss of noisy ISI channels due to narrow-band interference," *IEEE Communication Letters*, vol. 5, pp. 233 –235, Jun. 2001.

[2] Alamouti, S. M., "A simple transmit diversity technique for wireless communications," *IEEE Journal on Selected Areas in Communications*, vol. 16, Oct. 1998.

[3] Andersen, J. B., "Antenna arrays in mobile communications: gain, diversity, and channel capacity," *IEEE Antennas and Propagation Magazine*, vol. 42, pp. 12–16, Apr. 2000.

[4] Bellofiore, S., Foutz, J., Govindarajula, R., Bahceci, I., Balanis, C. A., Spanias, A. S., Capone, J. M., and Duman, T. M., "Smart antenna system analysis, integration and performance for mobile ad-hoc networks (MANETs)," *IEEE Transactions on Antennas and Propagation*, vol. 50, pp. 571–581, May 2002.

[5] Bliss, D., Forsythe, K. W., Hero, A. O., and Swindlehurst, A. L., "MIMO environmental capacity sensitivity," *Proc. of IEEE Asilomar Conference on Signals, Systems, and Computers*, vol. 1, Oct. 2000.

[6] Bliss, D., Forsythe, K. W., Hero, A. O., and Yegulalp, A. F., "Environmental issues for MIMO capacity," *IEEE Transactions on Signal Processing*, vol. 50, pp. 2128–42, Sep. 2002.

[7] Blum, R. S. and Winters, J. H., "On optimum MIMO with antenna selection," *IEEE Communication Letters*, vol. 6, pp. 322–324, Aug. 2002.

[8] Blum, R. S., Winters, J. H., and Sollenberger, N. R., "On the capacity of cellular systems with MIMO," *Proc. of the IEEE Vehicular Technology Conference*, vol. 2, Oct. 2001.

[9] Blum, R. S., Winters, J. H., and Sollenberger, N. R., "On the capacity of cellular systems with MIMO," *IEEE Communication Letters*, vol. 6, pp. 242–244, Jun. 2002.

[10] Bourk, T., "Techniques mitigate interference between 802.11 and Bluetooth." http://www.eetimes.com/in_focus/mixed_signals/OEG20021107S0022, Nov. 2002.

[11] C. Komninakis, C., Fragouli, C., Sayed, A. H., and Wesel, R. D., "MIMO transmission over a time-varying TDD channel using SVD," *IEEE Transactions on Signal Processing*, vol. 50, pp. 1065–1076, May 2002.

[12] Catreux, S., Driessen, P. F., and Greenstein, L. J., "Simulation results for an interference-limited multiple-input multiple output cellular system," *IEEE Communications Letters*, vol. 4, Nov. 2000.

[13] Chang, J.-H., Tassiulas, L., and Rashid-Farrokhi, F., "Joint transmitter receiver diversity for efficient space division multiaccess," *IEEE Transactions on Wireless Communications*, vol. 1, pp. 16–27, Jan. 2002.

[14] Chung, S. T., Lozano, A., and Huang, H. C., "Approaching eigenmode BLAST channel capacity using V-BLAST with rate and power feedback," *Proc. of the IEEE Vehicular Technology Conference*, vol. 2, 2001.

[15] Cover, T. M. and Thomas, J. A., *Elements of Information Theory*. Wiley, 1991.

[16] Dai, H. and Molish, A. F., "Multiuser detection for interference-limited MIMO systems," *Proc. of the IEEE Vehicular Technology Conference*, vol. 1, pp. 45–49, May 2002.

[17] Demirkol, M. F. and Ingram, M. A., "Power-controlled capacity for interfering MIMO links," *Proc. of the IEEE Vehicular Technology Conference*, vol. 1, pp. 187–191, Oct. 2001.

[18] Demirkol, M. F. and Ingram, M. A., "Control using capacity constraints for interfering MIMO links," *Proc. of the Int. Symp. on Personal, Indoor and Mobile Radio Communications*, vol. 3, pp. 1032–1036, Sep. 2002.

[19] Demirkol, M. F. and Ingram, M. A., "Stream control in networks with interfering MIMO links," *to appear in the Proc. of IEEE Wireless Communications and Networking Conference*, Mar. 2003.

[20] Edelman, A., *Eigenvalues and condition numbers of random matrices*. PhD thesis, Massachusetts Institute of Technology, Cambridge, MA, 1989.

[21] Farrokhi, F. R., Foschini, G. J., Lozano, A., and Valenzuela, R. A., "Link-optimal space-time processing with multiple transmit and receive antennas," *IEEE Communication Letters*, vol. 5, pp. 85–87, Mar. 2001.

[22] Farrokhi, F. R., Liu, K. J. R., and Tassiulas, L., "Transmit beamforming and power control for cellular wireless systems," *IEEE Journal on Selected Areas in Communications*, vol. 16, pp. 1437–1450, Oct. 1998.

[23] Farrokhi, F. R., Lozano, A., Foschini, G. J., and Valenzuela, R. A., "Spectral efficiency of wireless systems with multiple transmit and receive antennas," *Proc. of the IEEE Int. Symp. on Personal, Indoor and Mobile Radio Communications*, 2000.

[24] Foschini, G. J., "Layered space-time architecture for wireless communication in a fading environment when using multi-antenna elements," *Bell Labs Technical Journal*, 1996.

[25] Foschini, G. J. and Gans, M. J., "On limits of wireless communications in a fading environment when using multiple antennas," *Wireless Personal Communications*, vol. 6, pp. 311–335, 1998.

[26] Foschini, G. J. and Miljanic, Z., "A simple distributed autonomous power control algorithm and its convergence," *IEEE Transactions on Vehicular Technology*, vol. 42, pp. 641–646, Nov. 1993.

[27] Ge, H., Wong, K. D., Barton, M., and Liberti, J. C., "Statistical characterization of multiple-input multiple-output (MIMO)channel capacity," *IEEE Wireless Communications and Networking Conference*, vol. 2, pp. 789–793, 2002.

[28] Gill, P., Murray, W., and Wright, M. H., *Practical Optimization*. London: Academic Press, 1981.

[29] Godara, L. C., "Applications of antenna arrays to mobile communications, part I: performance inmprovement, feasibility, and system considerations," *Proceedings of the IEEE*, vol. 85, pp. 1031–1059, Jul. 1997.

[30] Golden, G. D., Foschini, G. J., Valenzuela, R. A., and Wolniansky, P. W., "Selecting an optimal set of transmit antennas for a low rank matrix channel," *Proc. of the 2000 IEEE International Conference on Acoustics, Speech, and Signal Processing*, vol. 5, pp. 2785–2788, Jan. 1999.

[31] Gore, D. A., Nabar, R. U., and Paulraj, A., "Detection algorithm and initial laboratory results using the V-BLAST space-time communication architecture," *Electronic Letters*, vol. 35, pp. 14–16, Jan. 1999.

[32] Hassibi, B. and Hochwald, B., "Optimal training in space-time systems," *Conference Record of the Asilomar Conference on Signals, Systems and Computers*, vol. 35, pp. 743–747, 2000.

[33] Haykin, S., *Communication Systems*. Wiley, 3 ed., 1994.

[34] Heath, R. W. and Paulraj, A., "Antenna selection for spatial multiplexing systems with linear receivers," *IEEE Communication Letters*, vol. 5, Apr. 2001.

[35] Heath, R. W. and Paulraj, A., "Characterization of MIMO channels for spatial multiplexing systems," *IEEE International Conference on Communications*, vol. 2, pp. 591–595, 2001.

[36] Hochwald, B. and Marzetta, T. L., "Space-time midulation for unknown fading," *Proc. of the SPIE Aerosense Conference*, Apr. 1999.

[37] Jiang, J.-S., Demirkol, M. F., and Ingram, M. A., "Measured capacities at 5.8 GHZ of indoor MIMO systems with interference," *submitted to the IEEE Vehicular Technology Conference*, Oct. 2003.

[38] Jiang, J.-S. and Ingram, M. A., "Path models and MIMO capacity for measured indoor channels at 5.8 GHZ," *Proc. of the Int. Symp. on Antenna Technology and Applied Electromagnetics*, Aug. 2002.

[39] Kang, M. and Alouini, M.-S., "Performance analysis of MIMO systems with co-channel interference over rayleigh fading channels," *Proc. of the IEEE International Conference on Communications*, vol. 1, pp. 391–395, Apr. 2002.

[40] Khatri, C. G., "Distribution of the largest or the smallest characteristic root under null hyperthesis concerning complex multivariate normal populations," *Ann. Math. Stat.*, vol. 35, pp. 1807–1810, Dec. 1964.

[41] Ko, Y., Shankarkumar, V., and Vaidya, N. H., "Medium access control protocols using directional antennas in ad hoc networks," *Proc. of the Annual Joint Conference of the IEEE Computer and Communications Societies INFOCOMM*, vol. 1, pp. 13–21, Mar. 2000.

[42] Laneman, J. N., Wornell, G. W., and Tse, D. N. C., "An efficient protocol for realizing cooperative diversity in wireless networks," *IEEE International Symposium on Information Theory*, p. 294, 2001.

[43] Lebrun, G., Ying, T., and Faulkner, M., "MIMO transmission over a time-varying tdd channel using svd," *Electronic Letters*, vol. 37, pp. 1363–1364, Oct. 2001.

[44] Li, K.-H., Ingram, M. A., and Nguyen, A. V., "Impact of clustering in statistical indoor propogation models on link capacity," *IEEE Transactions on Communications*, vol. 50, pp. 521–523, Apr 2002.

[45] Li, K.-H., Ingram, M. A., and Rausch, E., "Multibeam antennas for indoor wireless communications," *IEEE Transactions on Communications*, vol. 50, pp. 192 –194, Feb 2002.

[46] Li, Y. and Liu, K. J. R., "Blind identification and equalization for multiple-input/multiple-output channels," *Proc. of the IEEE Global Telecommunications Conference*, vol. 3, pp. 1789–1793, Nov. 1996.

[47] Liu, T.-Y. and Scholtz, R. A., "Link search algorithms for a spread-spectrum mobile communication network with directive/adaptive antennas," *Proc. of the IEEE Int. Conference on Communications*, vol. 2, pp. 1058–63, Jun. 1998.

[48] Marzetta, T. L., "BLAST training: estimating channel characteristics for high capacity space-time wireless," *Proc. of the Annual Allerton Conference on Communication, Control, and Computing*, Sep. 1999.

[49] Mehta, M. L., *Random matrices*. Boston: Academic Press, 2nd ed., 1991.

[50] Nam, S. H. and Lee, K. B., "Transmit power allocation for an extended V-BLAST system," *Proc. of the IEEE Int. Symp. on Personal, Indoor and Mobile Radio Communications*, Sep. 2002.

[51] Nasipuri, A., Ye, S., You, J., and Hiromoto, R. E., "A MAC protocol for mobile ad hoc networks using directional antennas," *Proc. of the IEEE Wireless Communications and Networking Conference*, vol. 3, pp. 1214–1219, 2000.

[52] Pahlavan, K. and Levesque, A., *Wireless Information Networks*. New York: John Wiley and Sons, 1995.

[53] Raleigh, G. G. and Cioffi, J. M., "Spatio-temporal coding for wireless communication," *IEEE Transactions on Communications*, vol. 46, Mar. 1998.

[54] Raleigh, G. G. and Jones, V. K., "Adaptive antenna transmission for frequency duplex digital wireless communication," *Proc. of the IEEE Int. Conference on Communications*, pp. 641–646, Mar. 1997.

[55] Rappaport, T. S., "Wireless personal communications: trends and challenges," *IEEE Antennas and Propagation Magazine*, vol. 33, pp. 19–29, Oct. 1991.

[56] Schittowski, K., "NLQPL: A FORTRAN-subroutine solving constrained nonlinear programming problems," *Annals of Operations Research*, vol. 5, pp. 485–500, 1985.

[57] Sendonaris, A., Erkip, E., and Aazhang, B., "Fading correlation and its effect on the capacity of multi-element antennas," *Proc. of the IEEE Int. Symposium on Information Theory*, p. 156, Aug. 1998.

[58] Sengupta, A. M. and Mitra, P. P., "Capacity of multivariate channels with multiplicative noise: I. random matrix techniques and large-n expansions for full transfer matrices," *Bell Labs Technical Report*, Apr. 2001.

[59] Shiu, D., Foschini, G. J., Gans, M. J., and Kahn, J. M., "Fading correlation and its effect on the capacity of multi-element antennas," *IEEE Transactions on Communications*, vol. 48, Mar. 2000.

[60] Silverstein, J. W., "The smallest eigenvalue of a large-dimensional Wishart matrix," *Ann. Probability*, vol. 13, pp. 1364–1368, 1985.

[61] Smith, P. J. and Shafi, M., "On a gaussian approximation to the capacity of wireless MIMO systems," *Proc. of the IEEE Int. Conference on Communications*, vol. 1, pp. 406–410, 2002.

[62] Spencer, Q. H., Jeffs, B. D., Jensen, M. A., and Swindlehurst, A., "Modeling the statistical time and angle of arrival characteristics of an indoor multipath channel," *IEEE Journal on Selected Areas in Communications*, vol. 18, pp. 347–360, Mar. 2000.

[63] Stüber, G. L., *Principles of Mobile Communication*. Boston: Kluwer Academic Publishers, 2nd ed., 2001.

[64] Sun, Q., Cox, D. C., Huang, H. C., and Lozano, A., "Estimation of continuous flat fading MIMO channels," *Proc. of the IEEE Wireless Communications and Networking Conference*, vol. 1, pp. 189–193, Mar. 2002.

[65] Sun, Q., Cox, D. C., Lozano, A., and Huang, H. C., "Training-based estimation for continuous flat fading BLAST," *Proc. of the IEEE International Conference on Communications*, vol. 1, pp. 325–329, 2002.

[66] Talwar, S., Viberg, M., and Paulraj, A., "Blind estimation of multiple cochannel digital signals using an antenna array," *IEEE Signal Processing Letters*, vol. 1, pp. 29–31, Feb. 1994.

[67] Tarokh, V., Jafarkhani, H., and Calderbank, A. R., "Space-time block codes from orthogonal designs," *IEEE Transactions on Information Theory*, vol. 45, pp. 1456–67, Jul. 1999.

[68] Tarokh, V., Jafarkhani, H., and Calderbank, A. R., "Space-time block coding for wireless communications: performance results," *IEEE Journal on Selected Areas in Communications*, vol. 17, pp. 451–460, Mar. 1999.

[69] Tarokh, V., Seshadri, N., and Calderbank, A. R., "Space-time codes for high data rate wireless communication: performance criterion and code construction," *IEEE Transactions on Information Theory*, vol. 44, pp. 744–765, Mar. 1998.

[70] Telatar, E., "Capacity of multi-antenna gaussian channels," *Technical Report, AT&T Bell Labs*, June 1995.

[71] Thompson, J. S., Grant, P. M., and Mulgrew, B., "Smart antenna arrays for CDMA systems," *IEEE Personal Communications*, pp. 16–25, Oct. 1996.

[72] Tsoulos, G. V., "Smart antennas for mobile communications: benefits and challenges," *Electronics and Communication Engineering Journal*, pp. 84–94, Apr. 1999.

[73] Verdu, S., "Wireless bandwidth in the making," *IEEE Communications Magazine*, pp. 53–58, Jul. 2000.

[74] Winters, J. H., "Smart antennas for wireless systems," *IEEE Personal Communications*, pp. 23–27, Feb. 1998.

[75] Winters, J. H. and Gans, M. J., "The range increase of adaptive versus phased arrays in mobile radio systems," *Proc. of IEEE Asilomar Conference on Signals, Systems, and Computers*, pp. 109–115, Oct. 1994.

[76] Winters, J. H., Salz, J., and Gitlin, R. D., "The impact of antenna diversity on the capacity of wireless communication systems," *IEEE Transactions on Communications*, vol. 42, no. 2, 1994.

[77] Zheng, H. and Samardzija, D., "Performance evaluation of indoor wireless systems using BLAST testbed," *Vehicular Technology Conference*, vol. 2, Oct. 2001.

VITA

Mehmet Fatih Demirkol was born in 1976 in Sanliurfa, Turkey. He received his B.S. degree University of Southern California, CA, USA, in May 1998, and his M.S. degree from Georgia Institute of Technology, GA, USA, in May 2000, both in Electrical and Computer Engineering. Since the spring of 2000, he has been pursuing the Ph.D. degree in the School of Electrical and Computer Engineering, Georgia Institute of Technology. His research interests include array signal processing, communication systems, networking, information theory, and random processes.